



1 **Wet deposition in the remote western and central Mediterranean**
2 **as a source of trace metals to surface seawater**

3 Karine Desboeufs¹, Franck Fu¹, Matthieu Bressac^{2,3}, Antonio Tovar-Sánchez⁴, Sylvain Triquet¹,
4 Jean-François Doussin⁵, Chiara Giorio^{6,7}, Patrick Chazette⁸, Julie Disnaquet^{9,10}, Anaïs Feron¹,
5 Paola Formenti¹, Franck Maisonneuve⁵, Araceli Rodríguez-Romero⁴, Pascal Zapf⁵, François
6 Dulac⁸ and Cécile Guieu³

7 ¹ Université de Paris and Univ Paris Est Creteil, CNRS, LISA, UMR 7583, F-75013 Paris, France

8 ² Institute for Marine and Antarctic Studies, University of Tasmania, Hobart, Tasmania, Australia.

9 ³ Laboratoire d'Océanographie de Villefranche (LOV), CNRS-Sorbonne Université, INSU, Villefranche-sur-Mer,
10 06230, France.

11 ⁴ Department of Ecology and Coastal Management, Institute of Marine Sciences of Andalusia (CSIC), 11510 Puerto
12 Real, Cádiz, Spain.

13 ⁵ Univ Paris Est Creteil and Université de Paris, CNRS, LISA, UMR 7583, F-94010 Créteil, France

14 ⁶ Laboratoire de Chimie de l'Environnement (LCE), UMR 7376 CNRS, Aix-Marseille Université, Marseille, 13331,
15 France.

16 ⁷ Yusuf Hamied Department of Chemistry, University of Cambridge, Lensfield Road, CB2 1EW, Cambridge, United
17 Kingdom

18 ⁸ Laboratoire des Sciences du Climat et de l'Environnement (LSCE), UMR 8212 CEA-CNRS-UVSQ, Institut Pierre-
19 Simon Laplace, Univ. Paris-Saclay, 91191 Gif-sur-Yvette, France.

20 ⁹ Marine Biology Research Division, Scripps Institution of Oceanography, UCSD, USA

21 ¹⁰ Sorbonne Université, CNRS, Laboratoire d'Océanographie Microbienne, LOMIC, France

22

23

24 *Correspondence to:* Karine Desboeufs (karine.desboeufs@lisa.ipsl.fr)

25

26

27

28

29

30



31 **Abstract.** This study reports the only recent characterisation of two contrasted wet deposition events
32 collected during the PEACETIME cruise in the Mediterranean open seawater, and their impact on
33 trace metals (TMs) marine stocks. Rain samples were analysed for Al, 12 trace metals (TMs
34 hereafter, including Co, Cd, Cr, Cu, Fe, Mn, Mo, Ni, Pb, Ti, V and Zn) and nutrients (N, P, DOC)
35 concentrations. The first rain sample collected in the Ionian Sea (rain ION) was a wet typical
36 regional background deposition event whereas the second rain collected in the Algerian Basin (rain
37 FAST) was a Saharan dust wet deposition. The concentrations of TMs in the two rain samples were
38 significantly lower compared to concentrations in rains collected at coastal sites reported in the
39 literature, suggesting either less anthropogenic influence in the remote Mediterranean environment,
40 or decreased emissions during the last decades in the Mediterranean Sea. The TMs inventories in
41 the surface microlayer and mixed layer (0-20m) at ION and FAST stations before and after the
42 events, compared to atmospheric fluxes, showed that the atmospheric inputs were a significant
43 source of particulate TMs for both layers. At the scale of the western and central Mediterranean, the
44 atmospheric inputs were of the same order of magnitude as marine stocks within the ML for
45 dissolved Fe, Co and Zn, underlining the role of the atmosphere in their biogeochemical cycle in
46 the stratified Mediterranean Sea. In case of intense wet dust deposition event, the contribution of
47 atmospheric inputs could be critical for dissolved stocks of the majority of TMs.



48 1. Introduction

49 Atmospheric deposition of continental aerosol has long been recognized to influence trace element
50 concentrations in remote oceanic surface waters (Buat-Ménard and Chesselet, 1979; Hardy, 1982;
51 Buat-Ménard, 1983). In particular, the Mediterranean Sea (Med Sea) is an oligotrophic environment
52 where marine biosphere growth is nutrient-limited during the long Mediterranean summer season
53 characterized by a strong thermal stratification of surface waters (The Mermex Group, 2011). The
54 Mediterranean atmosphere is characterized by the permanent presence of anthropogenic aerosols
55 from industrial and domestic activities around the basin (e.g., Sciare et al., 2003; Kanakidou et al.,
56 2011). In addition to this anthropogenic background, the Mediterranean basin is also subject to
57 seasonal contributions of particles from biomass fires in summer (Guieu et al., 2005) and to intense
58 sporadic Saharan dust inputs (e.g., Loÿe-Pilot and Martin, 1996; Vincent et al., 2016). Several
59 studies emphasized that the atmospheric deposition of aerosols, notably through wet deposition,
60 plays a significant role in marine cycles of both nutrient, such as nitrogen (N) and phosphorus (P)
61 (e.g. Pulido-Villena et al., 2010; Richon et al., 2018 a and b; Violaki et al., 2018) and micronutrients,
62 such as iron (Fe) (Bonnet and Guieu, 2006). Recently, atmospheric dust inputs were identified to
63 have a fertilizing effect on the plankton stocks and fluxes, even in the presence of relatively high
64 nutrients and Fe marine concentrations (Ridame et al., 2011; reviewed in Guieu and Ridame, 2021).
65 Mackey et al. (2012) showed that TMs provided by dust deposition could explain this fertilizing
66 effect. Indeed, some TMs, including Mn, Co, Ni (Mackey et al., 2012), Cu (Annett et al., 2008) and
67 Zn (Morel et al., 1991), play physiological roles for phytoplanktonic organisms. These TMs are
68 present in very low concentrations in oligotrophic systems such as the Med Sea, possibly limiting
69 the phytoplankton growth (Pinedo-González et al. 2015) and implying the role of dust deposition as
70 source of TMs for planktonic communities. On the other hand, atmospheric deposition of European
71 aerosol particles was identified to have a negative effect on chlorophyll concentrations (Gallisai et
72 al. 2014), by providing trace metals, as Cu, at toxic levels (Jordi et al. 2012).

73 The atmospheric deposition of TMs in the Mediterranean is related to both dust and anthropogenic
74 aerosols deposition (Desboeufs et al., 2018). The role of dust deposition as a source of TMs was
75 observed from the correlation between the atmospheric deposition of mineral dust, and the
76 enrichment of dissolved TMs (Cd, Co, Cu, Fe) in the Mediterranean Sea surface microlayer (Tovar-
77 Sánchez et al., 2014). For the water column, the adding of dissolved Fe and Mn was emphasized in
78 mesocosm experiments after dust addition mimicking intense wet dust deposition (Wuttig et al.,
79 2013). Yet, the direct impact of wet deposition events on TMs concentrations in surface seawater
80 has never been studied *in situ*, whether in the Mediterranean or in other oceanic regions. Moreover,



81 the two key criteria used to assess the potential impact of TMs and nutrients wet deposition are their
82 respective concentration (or flux) and solubility, i.e., the partitioning between dissolved and total
83 concentrations in rainwaters. Indeed, it is considered that the dissolved fraction of nutrients and
84 TMs can be directly assimilated by the phytoplankton. Few studies focussed on concentrations of
85 TMs in rainwater samples was collected around the Mediterranean basin: Al-Momani et al., (1998),
86 Kanellopoulou, (2001) and Özsoy and Örnektekin, (2009) in the eastern basin, and Losno (1989),
87 Guieu et al. (1997), Frau et al., (1996), Chester et al., (1997) and Guerzoni et al. (1999b) in the
88 western basin. These studies led to highly variable TMs concentration and solubility, illustrating a
89 more general large variability of TMs inputs during wet depositions in the Mediterranean Sea
90 (reviewed in Desboeufs, 2021). All these studies were performed at coastal sites. Offshore samples
91 of rainwater have rarely been studied in the literature so far. In the Mediterranean, to our knowledge,
92 trace element concentrations from only three rain samples collected at sea in April 1981 have been
93 reported in a PhD thesis (Dulac, 1986). However, due to the continental and local source of pollution
94 and the variety of anthropogenic aerosol sources (Amato et al., 2016), the TMs rain composition of
95 the coastal zone could not be representative of atmospheric deposition in the remote Mediterranean.

96 The PEACETIME cruise (ProcEss studies at the Air-sEa Interface after dust deposition in the
97 MEditerranean Sea) performed in spring 2017 aimed at studying the impacts of atmospheric
98 deposition, in particular Saharan dust events, on the physical, chemical and biological processes in
99 this marine oligotrophic environment (Guieu et al., 2020). We investigated here the concentration
100 and solubility of TMs and nutrients of two rainwaters sampled in the Mediterranean open sea during
101 the cruise. We compare our results on TMs concentrations and solubility in rainwater with previous
102 studies based on rainwater samples collected at coastal sites to investigate potential differences with
103 the open sea. Additionally, to assess the impact of wet deposition on the surface TMs
104 concentrations, surface seawater including the surface micro-layer was concurrently collected for
105 the first time with rain samples.

106 **2. Sampling and methods**

107 **2.1 Sampling and chemical analysis of rainwater**

108 The PEACETIME oceanographic campaign (<https://doi.org/10.17600/17000300>) took place in the
109 western and central Mediterranean Sea on-board the French research vessel (R/V) *Pourquoi Pas ?*
110 between 11 May and 10 June 2017, i.e. at the beginning of the Mediterranean stratification season
111 (Guieu et al., 2020). The rain collector was installed on the upper deck (22 m above sea level)



112 where no on-board activities were taking place to avoid contamination. A rain collector was
113 equipped with an on-line filtration system to directly separate the dissolved and particulate fractions
114 (details of the filtration system are available in Heimbürger et al., 2012) allowing for the calculation
115 of solubility of TMs in the rainwater at the time of collection. The filtration device was equipped
116 with a Nuclepore® polycarbonate membrane (PC) filter (porosity: 0.2 μm , diameter: 47 mm), and
117 the diameter of the funnel of the collector was 24 cm. The rain collectors were installed only when
118 rain was expected and kept closed within an acid-washed sealed plastic film until the rainfall began.
119 All the sampling materials were thoroughly washed in the laboratory prior to the cruise departure
120 (washing protocol described in Heimbürger et al., 2012). No stabilizing setup was used to keep the
121 funnel level during the pitch and roll of the ship, preventing a precise assessment of the height of
122 rainfall from the collected water volume. During the rain sampling, the ship was always facing the
123 wind to avoid contamination by the smoke of the ship itself, as the chimney was situated on the
124 lower deck and behind the collector.

125 Immediately after sampling, the collector was disassembled under the laminar flow hood inside a
126 clean-room on-board laboratory. The dissolved fraction was separated in 4 aliquots dedicated to i)
127 dissolved organic carbon (DOC) by high-temperature catalytic oxidation (HTCO) on a Shimadzu
128 total organic carbon analyzer (as described in Van Wambeke et al 2021), ii) major ions by ion
129 chromatography (IC), iii) metals analysis by inductively coupled plasma methods (ICP), and iv) pH
130 measurement. For ICP measurements, the sample was acidified immediately to 1% by volume of
131 ultra-pure nitric acid: 67-69%, Ultrapur, Normatom®, VWR. For IC analysis, the sample was
132 immediately frozen. The filter (particulate fraction) was dried under the laminar flow hood, and
133 then put in a storage box and packed with a plastic bag to avoid contamination. After returning to
134 the laboratory, filters were acid digested by using the adapted protocol from Heimbürger et al.
135 (2012) as follows: filters were placed in tightly capped Savillex™ PFA digestion vessels with 4 mL
136 of a mixture of HNO_3 (67-69%, Ultrapur, Normatom®, VWR), H_2O and HF acids (40%, Ultrapur,
137 Normatom®, VWR) in a proportion (3: 1: 0.5), then heated in an oven at 130°C for 14 hours. After
138 cooling, acid was completely evaporated on a heater plate (ANALAB, 250, A4) at 140°C for about
139 2h, then 0.5 mL of H_2O_2 (30-32%, Romil-UpA™) and 1 mL of the acidified water (2% HNO_3) was
140 added to the vessels and heated during 30 min. to dissolve the dry residue in the bottom of the
141 vessels; finally, 12 mL of acidified water (1% HNO_3) was added to obtain 13.5 mL of solution in a
142 tube for ICP-MS analyses.

143 The dissolved fraction was analysed by IC (IC 850 Metrohm) for the inorganic and organic anions
144 (NO_2^- , NO_3^- , PO_4^{3-} , SO_4^{2-} , F^- , Cl^- , Br^- , HCOO^- , CH_3COO^- , $\text{C}_2\text{H}_5\text{COO}^-$, MSA, $\text{C}_2\text{O}_4^{2-}$) and for the



145 cation NH_4^+ (Mallet et al., 2017). On the other hand, the dissolved fraction and solution from
146 digestion of particulate fractions were analysed by ICP-AES (Inductively Coupled Plasma Atomic
147 Emission Spectrometry, Spectro ARCOS Ametek®) for major elements (Al, Ca, K, Mg, Na, S)
148 (Desboeufs et al., 2014) and by HR-ICP-MS (High Resolution Inductively Coupled Plasma Mass
149 Spectrometry, Neptune Plus™ at Thermo Scientific™) for TMs: Cd, Co, Cr, Cu, Fe, Mn, Mo, Ni,
150 P, Pb, Ti, V and Zn. The speciation of dissolved P was estimated by determining the dissolved
151 inorganic phosphorus (DIP) from phosphate concentrations expressed as P and the dissolved
152 organic phosphorus (DOP) from the difference between total dissolved phosphorus (TDP), obtained
153 by ICP-MS, and DIP, obtained by IC.

154 In order to estimate the contamination of sampling and analytical protocols, 3 blanks of rain samples
155 (collected on-board during the cruise with the same protocol without rain events) were used and
156 processed. The procedural limit of detections (LoD) were defined as 3 x standard deviation of blank
157 samples both for dissolved and particulate fractions estimated after acid digestion. All samples
158 dissolved and particulate concentrations were higher than LoD, except for NO_2^- in the two rain
159 samples. The blank concentrations represented 10.2% in average for TMs and were typically lower
160 than 20% of the sample concentrations, except for Cd (52%) and Mo (43%) in the dissolved fraction.
161 For the sample concentration computations, we subtracted these blanks values to elemental
162 concentrations obtained in rain samples.

163 **2.2 Atmospheric ancillary measurements**

164
165 The PEGASUS (Portable Gas and Aerosol Sampling UnitS, www.pegasus.cnrs.fr) mobile platform
166 of LISA is a self-contained facility based on two standard 20-foot containers, adapted with air-
167 conditioning, rectified power, air intake and exhausts for sampling and online measurements of
168 atmospheric aerosols and gaseous compounds, and their analysis (Formenti et al., 2019). During the
169 PEACETIME cruise, only the sampling module of the facility was deployed on the starboard side
170 of deck 7 of the R/V. The PEGASUS instrumental payload of relevance to this paper included
171 measurements of the major gases such as NO_x , SO_2 , O_3 and CO by online analysers (Horiba APNA,
172 APSA, APOA and PICARRO respectively; 2-min resolution, detection limit 0.5 ppb and 1 ppb for
173 CO), that were used to estimate origins of collected air masses.

174 From the first of June (not operational before), additional measurements by an ALS450® Rayleigh-
175 Mie lidar (Leosphere™; Royer et al., 2011) was used to monitor the vertical distribution of aerosols
176 over time and the associated integrated columns. The vertical lidar profiles were analysed to yield
177 the apparent backscatter coefficient (ABC) corrected from the molecular transmission, as well as



178 the volume depolarisation ratio (VDR). The inversion procedure (Chazette et al., 2016; 2019) to
179 retrieve the aerosol extinction coefficient (unit km^{-1}) uses a vertical-dependent lidar ratio that takes
180 into account two aerosol layers. The first layer corresponds to marine aerosols in the marine
181 boundary layer (MBL), the second to a desert aerosol layer that can extend between ~ 1 and 6 km
182 above mean sea level (amsl). In accordance with Chazette et al. (2016), for the same wavelength
183 and region, the lidar ratios were set to 25 and 55 sr, respectively. The vertical profile of the aerosol
184 extinction coefficient was retrieved from 0.2 km amsl on with a vertical resolution of 15 m. Based
185 on these profiles, the integrated column content of dust aerosols was estimated using a specific
186 extinction cross-section of $1.1 \text{ m}^2 \text{ g}^{-1}$ as proposed by Raut and Chazette (2009).

187 In addition, detailed meteorological data such as air and sea temperature, atmospheric pressure,
188 relative humidity, atmospheric pressure, heat flux and wind speed and direction were provided on
189 a 30 seconds timestep basis by the ship's permanent instrumentation.

190 **2.3 Sampling and analysis of dissolved TMs in seawater**

191 Before and after each rain, seawater samples were collected in the surface microlayer (SML: <1
192 mm) and subsurface seawater (SSW: <1 -m depth) (Tovar-Sánchez et al., 2020, this special issue).
193 SML and SSW samples were collected from a pneumatic boat 0.5-1 nautical mile away from the
194 R/V in order to avoid any potential contamination. SML samples were collected using a glass plate
195 sampler (Stortini et al., 2012; Tovar-Sánchez et al., 2019) which had previously been cleaned with
196 acid overnight and rinsed thoroughly with ultrapure water (MQ-water). The 39 x 25 cm silicate
197 glass plate had an effective sampling surface area of 1950 cm^2 considering both sides. In order to
198 check for procedural contamination, SML blanks were collected at some stations on board of the
199 pneumatic boat by rinsing the glass plate with ultra-pure water and collecting 0.5 L of ultra-pure
200 water using the glass plate system. The surface microlayer thickness was calculated following the
201 formula of Wurl (2009). SSW was collected by using an acid-washed Teflon tubing connected to a
202 peristaltic pump. The total fraction (i.e. T-SML) was directly collected from the glass plate system
203 without filtration in a 0.5 L acid cleaned LDPE bottles, while the dissolved fraction in the SML (i.e.
204 D-SML) and SSW (i.e. D-SSW) was filtered in situ through an acid-cleaned polypropylene cartridge
205 filter ($0.22 \mu\text{m}$; MSI, Calyx®).

206 TMs samples were also collected in the water column using the trace metals clean (TMC) rosette
207 before and after the rains (Bressac et al., 2021). Although rosette deployments were performed over
208 the whole water column, we focus here on the 0-20 m marine mixed-layer (ML). The water column
209 was sampled using the TMC titanium rosette mounted with 24 teflon-coated Go-Flo bottles.



210 Immediately after recovery, the Go-Flo bottles were transferred inside a class-100 clean laboratory
211 container. Seawater samples were directly filtered from the bottles through acid-cleaned 0.2- μm
212 capsule filters (Sartorius Sartobran-P-capsule 0.45/0.2- μm). All samples were acidified on board to
213 pH <2 with Ultrapure-grade HCl under a class-100 HEPA laminar flow hood. Metals (namely Cd,
214 Co, Cu, Ni, Mo, V, Zn and Pb) were pre-concentrated using an organic extraction method (Bruland
215 et al., 1979) and quantified by ICP-MS (Perkin Elmer ELAN DRC-e). In order to breakdown metal-
216 organic complexes and remove organic matter (Achterberg et al., 2001; Milne et al., 2010), total
217 fraction samples (i.e. T-SML) were digested prior to the pre-concentration using a UV system
218 consisting of one UV (80 W) mercury lamp that irradiated the samples (contained in quartz bottles)
219 during 30 min. The accuracy of the pre-concentration method and analysis for TMs was established
220 using Seawater Reference Material (CASS 6, NRC-CNRC) with recoveries ranging from 89% for
221 Mo to 108% for Pb. Due to the complexity of the analytical method, all the TMC samplings were
222 not analysed for these metals. Overall, 1 or 2 depths were obtained in the mixed layer (0-20 m).
223 Dissolved Fe and Al concentrations were also measured on board. Dissolved Fe concentrations were
224 measured using an automated Flow Injection Analysis (FIA) with online preconcentration and
225 chemiluminescence detection (Bonnet and Guieu, 2006), and dissolved Al concentrations using the
226 fluorometric method described by Hydes and Liss (1976). Sampling and analysis for dissolved Fe
227 and Al concentrations are fully described in Bressac et al. (2021), and covered at least 4 depths in
228 the 0-20 m mixed layer.

229 **2.4 Enrichment factor and solubility**

230 In order to better constrain the origin of TMs in the rain samples, their enrichment factor (EF; Rahn
231 1976) relative to the Earth's crust was calculated based on their total concentrations (dissolved +
232 particulate fractions) as:

$$233 \quad EF = \frac{([X]/[Al])_{sample}}{([X]/[Al])_{crust}} \quad (1)$$

234 where $[X]/[Al]$ is the ratio between an element X and Al concentrations in rainwater samples (at
235 the numerator), and in the Earth's crust (denominator) from Rudnick and Gao (2003). Aluminium
236 is currently used as a reference element as it only has a crustal origin. For a given TM, $EF > 1$
237 indicates an enrichment with respect to the average composition of the Earth's crust. To account for
238 the soil composition variability of mineral dust atmospheric sources, TMs with an EF value > 10 are
239 considered derived from non-crustal sources (Rahn, 1976).

240 The relative solubility of TMs in the two rainwater events was calculated as:



241
$$S_X\% = \frac{[X]_{dissolved}}{[X]_{total}} \times 100 \quad (2)$$

242 where $S_X\%$ is the relative solubility (in %) of an element X in the rainwater, $[X]_{dissolved}$ and $[X]_{total}$
243 are its soluble and total concentration, respectively.

244 **2.5 Atmospheric deposition fluxes**

245 Impacts on biogeochemical cycles and ecosystem functioning after a rain event occur on time scales
246 of a few days (2-3), and space scales of tens of km (about 20-50 km within the radius of the ship's
247 position). In the specific context of oceanographic cruising, the documentation of these impacts is
248 restricted to the vertical dimension at the prescribed temporal scale. In this vertical dimension, the
249 exchange of TMs across the ML was controlled both by atmospheric inputs over the R/V position
250 and by advection from surrounding water masses that may have been impacted by surrounding
251 rainfall. Therefore, we had to consider this process in our estimation of the atmospheric fluxes
252 contributions. For this purpose, the atmospheric fluxes have to be integrated to the extent of the rain
253 area that can impact the marine surface layers. We derived wet deposition fluxes by considering the
254 total precipitation accumulated during the duration of the rain over the area around the R/V location.
255 Thus, the wet deposition fluxes in our rain samples were calculated by multiplying the volume
256 weighted mean rainfall concentration by the total precipitation. The total precipitation of the rain
257 events was issued from the hourly total precipitation accumulated during the rain events over the
258 region from ERA5 ECMWF reanalysis (Herbasch et al., 2018) and from the rain rate composite
259 radar products from the European OPERA database (Saltikoff et al., 2019), when it is possible.
260 Although subject to uncertainties (Morin et al., 2003), a surface-based weather radar is probably the
261 best tool to estimate rainfall in the surroundings of the R/V. However, the OPERA database does
262 not include Italian radars, which anyway did not cover the central area of the Ionian Sea during the
263 cruise. ERA5 data are available on regular latitude-longitude grids at $0.25^\circ \times 0.25^\circ$ resolution. The
264 accumulated precipitation was taken from the grid-points spanning the ship's location, more or less
265 0.25° around the central grid-point for integrating the regional variability. Surface rain rate radar
266 composite images were available every 15 minutes with a spatial resolution of 2 km x 2 km. The
267 accumulated precipitation was the sum of integral rain rates during the rain duration averaged over
268 the radar pixels spanning the ship location within a radius of about 25 km around the ship location.

269 **2.6 Stocks in the surface seawater**

270 For the surface microlayer (SML), stocks of TMs were estimated from the integration of TMs
271 concentration over the thickness of the layer. The thickness ranged from 32 to 43 μm and from 26
272 to 43 μm at ION and FAST, respectively (Tovar-Sanchez et al., 2020).



273 The trace metals stocks within the ML were calculated by trapezoidal integrations of marine
274 concentrations from SSW and TMC rosette samplings. The upper water column was stratified along
275 the cruise transect (Taillandier et al., 2020), with a ML ranging from 7 to 21 m (11 to 21 m at ION
276 station and 11 to 19 m at FAST station (Van Wambeke et al., 2020). The ML depth (MLD)
277 fluctuations, for example due to wind peaks associated with rain events, could create rapidly
278 changing conditions of vertical advection from deeper waters. However, with no significant increase
279 in TMs concentrations being observed below the ML down to about 50 m (not shown), the
280 enrichment observed in the ML after rainfalls could not be attributed to any mixing with deeper
281 water due to high wind. In consequence, stocks in the ML have been integrated over a constant
282 depth range of 0-20 m for comparison, as Bressac et al. (2021). For Cu, Fe, Ni, Zn, stocks were
283 estimated both for the dissolved and particulate fractions in the SML and ML, for Co, Cd, Mo, Pb
284 and V for the dissolved fraction only in the ML and for both fractions in the SML and for Mn and
285 Ti only for the particulate fraction in the ML.

286 The partitioning coefficient between the particulate and dissolved phases (K_d
287 $=[\text{particulate}]/[\text{dissolved}]$) was used to investigate exchanges between dissolved and particulate
288 pools of TMs.

289 3. Results

290 3.1 General conditions

291 The general meteorological conditions during the cruise indicated that the ION and FAST stations
292 were highly affected by cloudy weather conditions. During these periods, 2 significant rains
293 occurred on the R/V position and have been collected: The first rain (hereafter Rain ION) was
294 collected during the 4-day ION station in the Ionian Sea in the early morning of 29/05 at 03:08
295 UTC, and the second rain (hereafter Rain FAST) occurred during the 5-day "Fast action" station,
296 (hereafter 'FAST') in the Algerian Basin during the night of 05/06 at 00:36 UTC (Table 1). The two
297 rain samples coincide with peaks in relative humidity and wind speed, and minima in air
298 temperature (not shown).

299 **Table 1: Information regarding the two rains collected during the PEACETIME cruise.**

Sample	Sampling time	Station name (dates) and rain location	Estimated total precipitation
--------	---------------	-------------------------------------------	----------------------------------

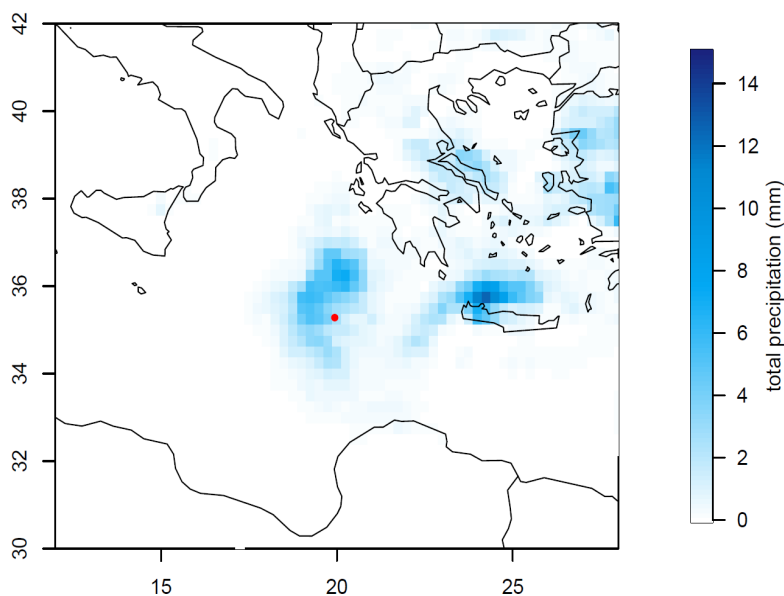


Rain ION	29 May 2017, 03:08–04:00 (UTC) 05:08–06:00 (local time)	ION (25–29 May) 35.36°N, 19.92°E	3.5 ±1.2 mm
Rain FAST	05 June 2017, 00:36–01:04 (UTC) 02:36–03:04 (local time)	FAST (2–7 June) 37.94°N, 2.91°E	6.0 ±1.5 mm

300

301 *3.1.1. Rain ION*

302 The ERA 5 data reanalysis shows 2 periods of precipitation in the surrounding of the ship's position,
303 i.e. in the morning and evening of June 26 (not shown) and in the night between June 28 and 29, in
304 agreement with on-board visual observations. The rain event collected at ION was the product of a
305 large cloud system, covering an area of about 90 000 km² around the R/V position, spreading over
306 the Ionian and Aegean Seas (Fig. 1). No radar measurements being available for this area, the
307 accumulated rate was estimated from ERA 5 data reanalysis on the grid-point corresponding to the
308 ION station and was 3.5 ±1.2 mm around the R/V position (±0.25°). The wash-out of the
309 atmospheric particles was revealed by the decrease in aerosol number concentrations monitored on-
310 board from about 1900 to 300 part.cm⁻³ (supplementary material Fig. S1). Air mass back-trajectories
311 showed that the scavenged air masses came from Greece both in the marine boundary layer and in
312 the free troposphere (Fig. S1). The satellite observations showed low aerosol optical thickness
313 during this period (not shown), meaning low amounts of aerosols in the atmospheric column. No
314 significant European pollution influence was monitored by on-board measurements during this
315 event, with major gas mixing ratio and aerosol concentrations in the average values of the cruise
316 (Fig. S1) and typical of clean atmospheric concentrations, i.e. under detection limit for NO_x, 1.2
317 ppb for SO₂, 51 ppb for O₃, 80 ppb for CO and 3000 part.cm⁻³. On this basis, this wet event was
318 representative of a Mediterranean background marine rain event.



319

320 **Figure 1: Total precipitation (mm) between May 28 at 20:00 UTC and 29 at 10:00 UTC from ERA5**
321 **ECMWF reanalysis. The red circle indicates the R/V position.**

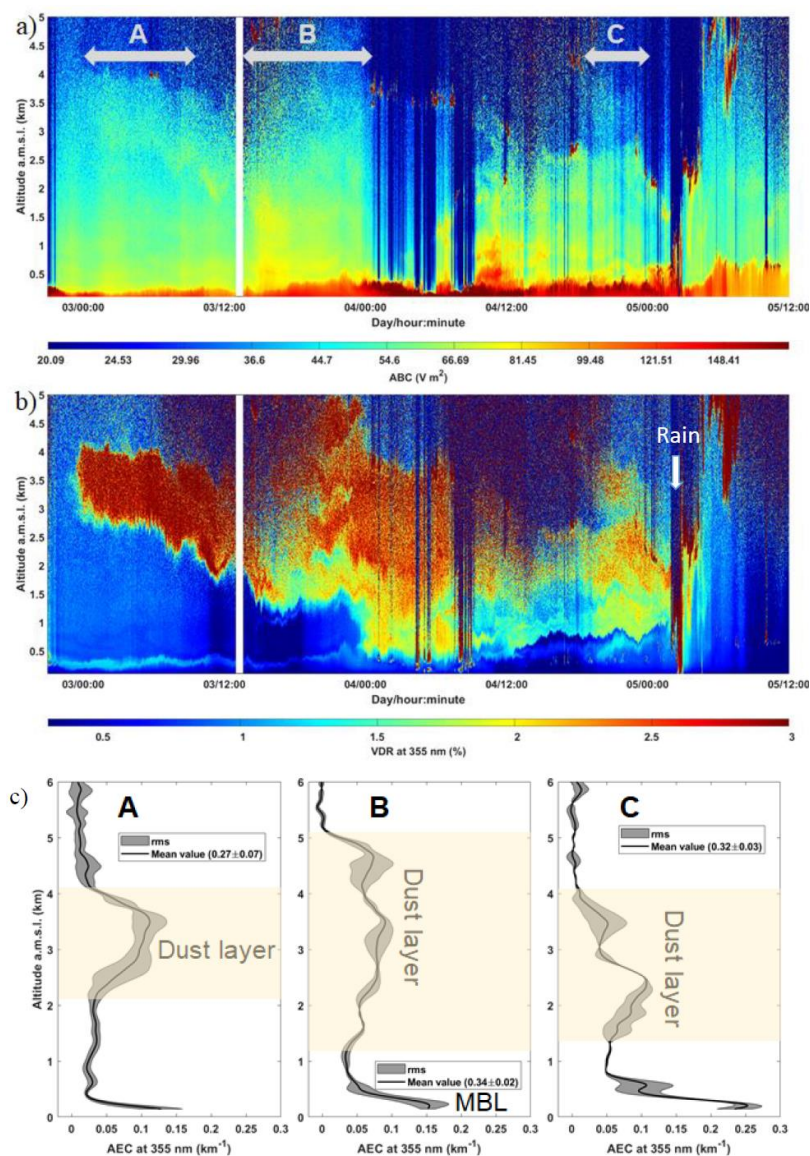
322 *3.1.2. Rain FAST*

323 As detailed in Guieu et al. (2020), the FAST station position was decided on the basis of regional
324 model forecast runs and satellite observations, in the purpose to catch a wet dust deposition event.
325 Significant dust emissions were observed from NASCube (<http://nascube.univ-lille1.fr/>, Gonzales
326 and Briottet, 2017) over North Africa from the night of 30-31 May, then new dust emissions in the
327 night from 3 to 4 June in Algeria and southern Morocco associated with a northward atmospheric
328 flux. On 30 May, the SEVIRI AOD satellite product ([https://www.icare.univ-lille.fr/data-
329 access/browse-images/geostationary-satellites/](https://www.icare.univ-lille.fr/data-access/browse-images/geostationary-satellites/), Thieuleux et al., 2005) confirmed the presence of
330 atmospheric dust in a cloudy air mass over the western part of the Mediterranean, and from 2 June
331 the export of a dust plume from North Africa south of the Balearic Islands with high AOD (>0.8)
332 on the Alboran Sea was observed (Fig. S2). The dust plume was transported to the NE up to Sardinia
333 on June 4, with AOD<0.5 in all the area and clear sky with low AOD was left west of 4°E on June
334 5.

335 On-board lidar measurements (Fig. 2 a,b,c) showed that the aerosol plume was present over the ship
336 position from 2 June at 21:00 UTC until the rain event, and corresponded to a dust aerosol layer
337 well highlighted by the high depolarization. The dust plume was concentrated between 3 and 4 km



338 at the beginning of the station, then expanded to the end of the day on June 3 down to the marine
 339 boundary layer (about 500 m amsl). The mass integrated contents of dust aerosols derived from the
 340 profiles of aerosol extinction ranged from a minimum of $0.18 \pm 0.005 \text{ g m}^{-2}$ just before the rain to a
 341 maximum of $0.24 \pm 0.009 \text{ g m}^{-2}$, where standard deviations indicate the temporal variability (1
 342 sigma).

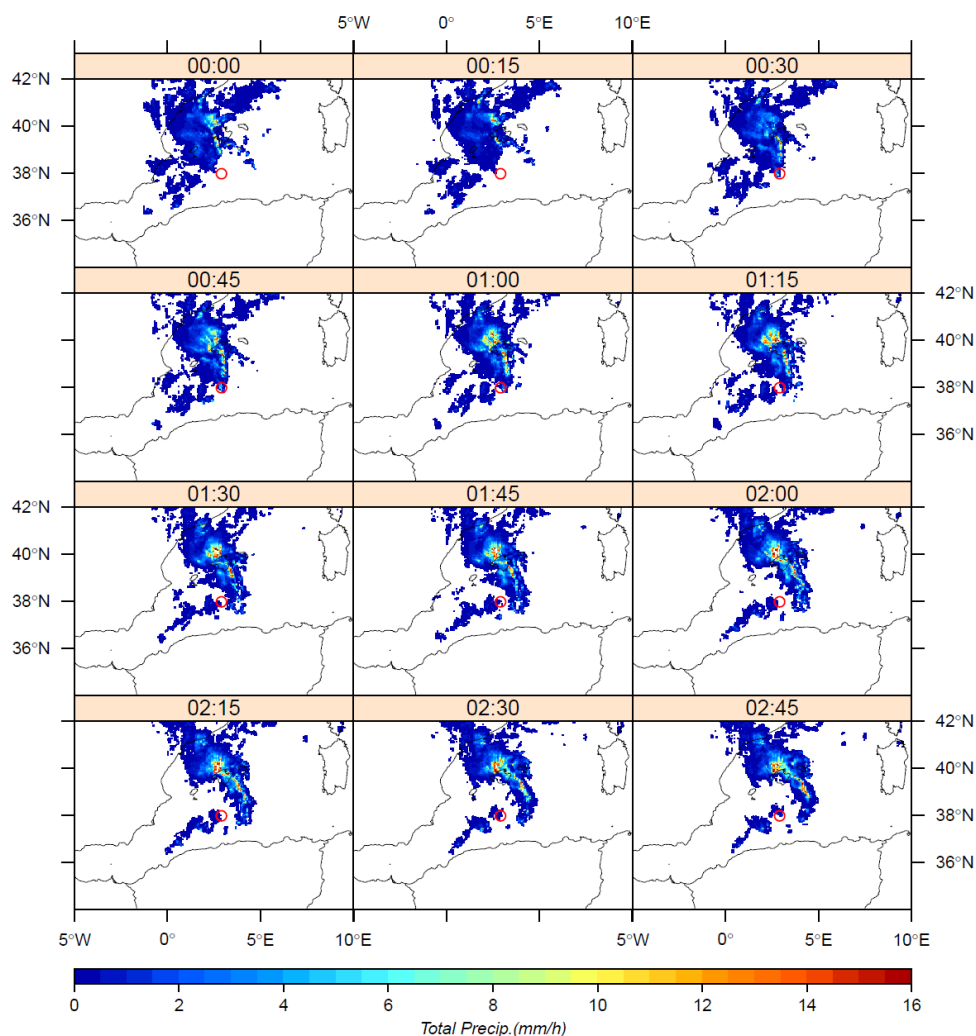


343



344 **Figure 2: On-board lidar-derived a) Apparent backscatter coefficient (ABC), (b) Temporal evolution**
345 **(in Local Time) of the lidar-derived volume depolarization ratio (VDR) where the dust plume is**
346 **highlighted for values higher than ~1.7 (yellow to red colors) and the rain by values higher than 3**
347 **(indicated by the arrow), and c) vertical profiles of the aerosol extinction coefficient (AEC) in cloud**
348 **free condition, integrated over 3 periods along the dust plume event, noted A, B and C in figure a. The**
349 **grey shade represents the root mean square (rms) variability along the time of the measurement. The**
350 **dust layer is highlighted on the profiles. The mean aerosol optical thickness is given in the boxed legend**
351 **with its temporal variability (1 sigma). The location of the marine boundary layer (MBL) is also**
352 **pointed.**

353 Rainfalls were observed by weather radar images in the neighbouring area of the R/V from 3 June
354 at 7:00 UTC. The rainfalls recorded around FAST station were associated with 2 periods of rain:
355 the 03/06 from 7:00 to 14:00 UTC, and from the 04/06 at 16:00 UTC to 05/06 at 06:00 UTC. For
356 this latter, a rain front (100 000 km²), moving eastward from Spain and North Africa regions,
357 reached the FAST station the night between the 4 and 5 June (Fig. 3). Wet deposition between the
358 4 and early 5 June in the FAST station area were confirmed by radar imagery, showing several other
359 rain spots around the R/V position before and after the rain sampling (Fig. 3). Continuous on-board
360 lidar measurements confirmed the below-cloud deposition during the rain event of early 5 June (Fig.
361 2b). Rain FAST was a wet deposition event occurring at the end of an episode of transport of
362 Saharan dust, whereas precipitation of the 3 June occurred during the maximum of the dust plume
363 (Fig. 2b and S2). The surface concentrations of gas and particles, measured on-board, suggest no
364 clear dust or anthropogenic influence in the atmospheric boundary layer during the period of wet
365 deposition, in agreement with back trajectories of low altitude air masses (Fig S2.), presuming no
366 local mixing between dust and anthropogenic particles into rain samples. The total precipitation
367 estimated from radar rainfall estimates yield an accumulated precipitation of 6.0 ± 1.5 mm (± 25 km
368 around), in agreement with ECMWF reanalysis ERA5 (Fig. S2) for the wet deposition on the night
369 of 4-5 June (5.7 ± 1.4 mm in the grid-point spanning the R/V position, i.e. $\pm 0.25^\circ$ around).



370

371 **Figure 3: Rain rates (mm/h) during the night between the 4 and 5 June, when Rain Fast has been**
372 **collected on board, issued from European rain radar composites (OPERA programme) of June 5**
373 **between 00:00 and 02:45 UTC.**

374 **3.2. Chemical composition of rains**

375 Dissolved and total concentrations of nutrients and TMs in the rain samples are presented in Table
376 2. Among all measured dissolved concentrations, NO_3^- was the most abundant nutrient, followed
377 by ammonium (Table 2). The nitrite concentration was under the limit of detection for the two rain
378 samples. Regarding TMs in rain, Fe and Zn presented the highest concentrations in rain samples
379 with the same order of magnitude (10 to 25 $\mu\text{g L}^{-1}$). Co, Cd and Mo had the lowest concentrations



380 (<0.1 $\mu\text{g L}^{-1}$ in both events), whereas the other TMs concentrations ranged between 0.1 and 10 μg
 381 L^{-1} in both rains (Table 2). Concentrations of nutrients and the majority of TMs were higher in the
 382 dust-rich rain, except Pb (similar concentrations in both rains) and Cr (3 times higher concentration
 383 in Rain ION relative to Rain FAST).

384 **Table 2: Dissolved and total concentrations of nutrients and TMs in the two rains collected during the**
 385 **PEACETIME cruise in $\mu\text{g.L}^{-1}$ or ng.L^{-1} and $\mu\text{mol.L}^{-1}$ or nmol.L^{-1} in the parentheses (sd = standard deviation**
 386 **from three replicates).**

		Rain ION				Rain FAST				
		Dissolved		Total		Dissolved		Total		
		concentrations	$\pm\text{sd}$	concentrations	$\pm\text{sd}$	concentrations	$\pm\text{sd}$	concentrations	$\pm\text{sd}$	
Nutrients	NO_3^-	$\mu\text{g L}^{-1}$ ($\mu\text{mol L}^{-1}$)	1185 (19.1)	71 (1.1)			3694 (59.6)	222 (3.6)		
	NH_4^+	$\mu\text{g L}^{-1}$ ($\mu\text{mol L}^{-1}$)	366 (20.3)	11 (0.6)			654 (36.3)	19 (1.1)		
	DIN	$\mu\text{g L}^{-1}$ ($\mu\text{mol L}^{-1}$)	552 (39.4)	82 (1.7)			1343 (96)	241 (17)		
	PO_4^{3-}	$\mu\text{g L}^{-1}$ (nmol L^{-1})	18.1 (189)	0.5 (6)			19.0 (200)	0.6 (6)		
	DIP	$\mu\text{g L}^{-1}$ (nmol L^{-1})	5.87 (189)	0.18 (6)			6.20 (200)	0.19 (6)		
	DOP	$\mu\text{g L}^{-1}$ (nmol L^{-1})	8.63 (278)	1.94 (75)			4.91 (158)	1.56 (57)		
	TP	$\mu\text{g L}^{-1}$ (nmol L^{-1})	14.51 (468)	2.52 (81)	16.6 (536)	1.0 (33)	11.11 (358)	1.95 (63)	58.7 (1894)	3.5
	DIN/DIP		(208)				(480)			
	DOC	($\mu\text{mol L}^{-1}$)	(105.7)	(2.2)			(95.5)	(1.2)		
Metals	Al	$\mu\text{g L}^{-1}$ (nmol L^{-1})	13.0 (480)	0.8 (30)	14.6 (540)	0.9 (32)	23.4 (867)	0.7 (24)	440 (16308)	7
	Cu	$\mu\text{g L}^{-1}$ (nmol L^{-1})	0.71 (11.1)	0.02 (0.3)	0.73 (11.5)	0.02 (0.3)	1.15 (18.0)	0.04 (0.6)	1.63 (25.7)	0.06
	Fe	$\mu\text{g L}^{-1}$ (nmol L^{-1})	15.1 (270)	0.4 (6)	17.9 (321)	0.6 (11)	19.2 (344)	0.1 (2)	231 (4140)	7
	Mn	$\mu\text{g L}^{-1}$ (nmol L^{-1})	0.55 (10.0)	0.02 (0.3)	0.60 (10.9)	0.02 (0.4)	3.17 (57.8)	0.07 (1.2)	5.26 (95.7)	0.12
	Ni	$\mu\text{g L}^{-1}$ (nmol L^{-1})	0.52 (8.8)	0.02 (0.3)	0.67 (11.4)	0.02 (0.4)	0.59 (10.1)	0.02 (0.4)	0.84 (14.3)	0.03
	Ti	$\mu\text{g L}^{-1}$ (nmol L^{-1})	0.48 (10.0)	0.04 (0.8)	0.65 (13.6)	0.48 (3.2)	0.22 (4.7)	0.01 (0.1)	33.36 (697)	0.51
	V	$\mu\text{g L}^{-1}$ (nmol L^{-1})	0.37 (7.4)	0.01 (0.2)	0.38 (7.42)	0.01 (0.25)	1.37 (26.9)	0.03 (0.5)	2.02 (39.7)	0.04
	Zn	$\mu\text{g L}^{-1}$ (nmol L^{-1})	24.8 (379)	0.8 (12)	25.3 (387)	0.8 (12)	22.7 (347)	0.6 (8)	26.3 (402)	0.7
	Cd	$\mu\text{g L}^{-1}$ (pmol L^{-1})	12.9 (115)	6.4 (57)	13.1 (117)	6.3 (56)	20.2 (180)	10.3 (92)	23.7 (210)	6.8
	Co	ng L^{-1} (pmol L^{-1})	44 (749)	13 (229)	47.4 (804)	14.5 (246)	82 (1386)	20 (347)	157 (2661)	28
	Cr	ng L^{-1} (pmol L^{-1})	241 (4636)	16 (300)	628 (12079)	5 (95)	79 (1522)	14 (260)	443 (8514)	43
	Mo	ng L^{-1} (pmol L^{-1})	28 (288)	10 (106)	4.1 (43)	1.4 (14)	82 (855)	11 (113)	92.1 (960)	16.2
	Pb	ng L^{-1} (pmol L^{-1})	170 (822)	11 (54)	175.1 (845)	1.4 (7)	166 (801)	9 (41)	604 (2917)	19

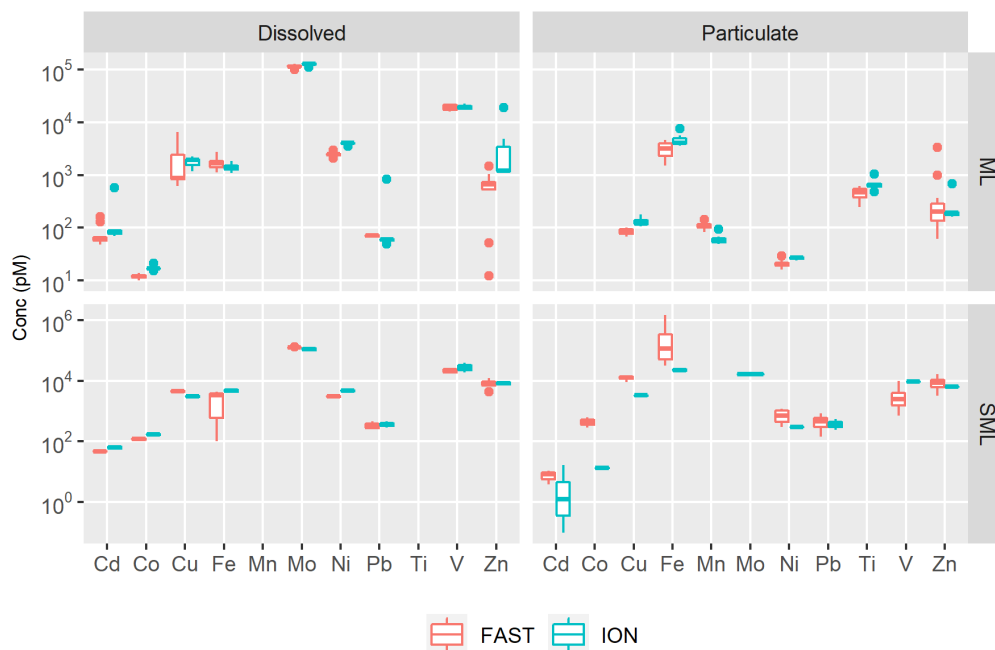
387

388 3.3. Marine concentrations and stocks

389 All the TMs had significantly higher concentrations in the ML compared to deep water masses, in
 390 agreement with a stratified profile associated with atmospheric input. The particulate and dissolved
 391 trace metal concentrations within the ML (0-20 m) and the SML are displayed in Fig. 4.
 392 Concentrations were of the same order of magnitude in the two studied stations, except for the
 393 particulate phase in the SML where the concentrations of Cu and Co were significantly lower at
 394 ION station. The TMs were mainly in dissolved forms in the ML, except for Fe, whose dissolved
 395 and particulate concentrations were in the same order of magnitude. On the contrary, the particulate
 396 phase contribution dominated for TMs in the SML, in particular at the ION station. At both stations,
 397 the highest TMs concentrations in the surface seawater were found for Mo in the dissolved fraction,



398 in agreement with the abundance of dissolved Mo in seawater (Smedley and Kinniburgh, 2017),
399 and Fe in the particulate fraction. All the particulate and dissolved TMs concentrations measured
400 during the cruise were representative for the Mediterranean Sea (Sherrell and Boyle, 1988; Saager
401 et al., 1993; Morley et al., 1997; Yoon et al., 1999; Wuttig et al., 2013; Baconnais et al., 2019;
402 Migon et al., 2020). Zn presented the largest range of concentrations within the ML both in the
403 particulate and dissolved phases, due to some high concentrations. However, the concentrations
404 stayed in the typical range of values found in the Mediterranean Sea (Bethoux et al., 1990, Yoon et
405 al., 1999). In the SML, the concentrations were lower than in the ML and Pb dominated both in
406 dissolved and particulate phases. Tovar-Sanchez et al. (2020) showed that the TMs concentrations
407 in the SML during the PEACETIME campaign were generally lower than those previously
408 measured in the Mediterranean Sea, except in the particulate phase during the FAST station after
409 dust deposition.



410
411 **Figure 4: Boxplots of dissolved (left panels) and particulate (right panels) marine concentrations (pM)**
412 **for the different TMs within the ML (upper panels) and the SML (lower panels) at ION and FAST**
413 **stations. In the box plots, the box indicates the interquartile range, i.e. the 25th and the 75 th percentile,**
414 **and the line within the box marks the median. The whiskers indicate the quartiles ± 1.5 times the**
415 **interquartile range. Points above and below the whiskers indicate outliers outside the 10 th and 90th**
416 **percentile.**

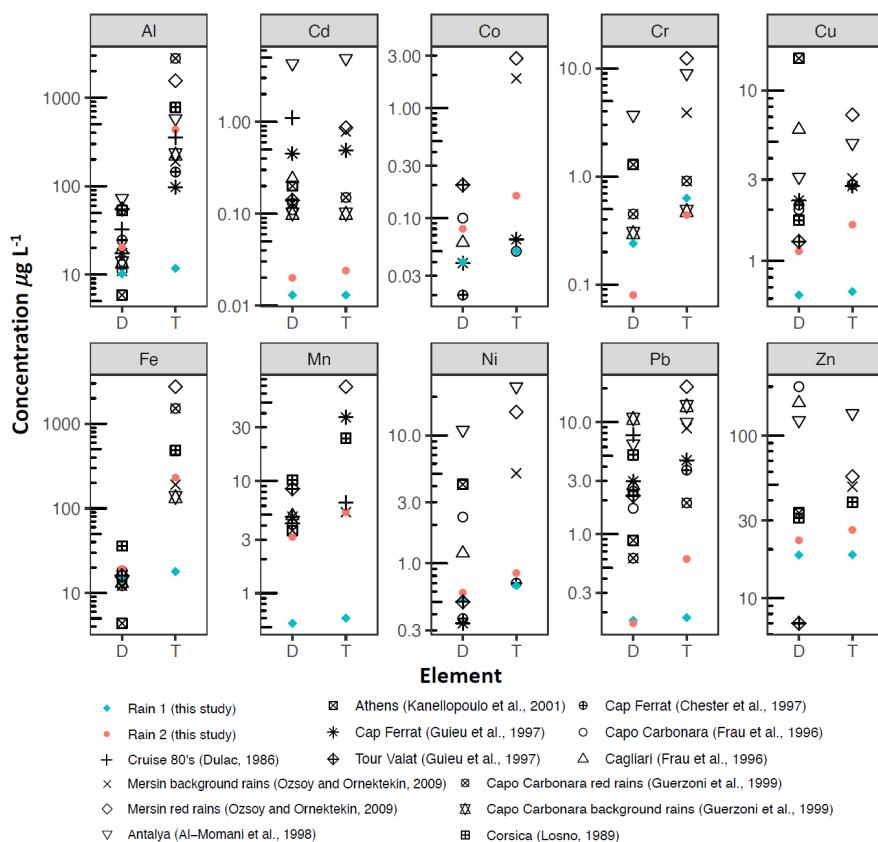


417 **4. Discussion**

418 **4.1. Composition of rain collected over the remote Med Sea**

419 *4.1.1. Concentrations*

420 Regarding nutrients, nitrogen species concentrations in rain samples were in good agreement with
421 those reported in Mediterranean rain samples, ranging from 1130 to 5100 $\mu\text{g L}^{-1}$ for NO_3^- and
422 between 207 and 1200 $\mu\text{g L}^{-1}$ for NH_4^+ (Loye-Pilot et al., 1990; Avila et al., 1997; Al Momani et
423 al., 1998; Herut et al., 1999; Violaki et al., 2010; Izquieta-Rojano et al., 2016; Nehir and Koçak,
424 2018). The FAST rain concentrations were in the average values, whereas the ION rain was in the
425 low range, confirming a background signature. The rainwater samples presented a large dominance
426 of N in comparison to P, as observed from the N/P ratio derived from DIN/DIP (Table 2) ranging
427 from 208 at ION to 480 at FAST. Previous observations showed a predominance of N relative to P
428 in the atmospheric bulk deposition over the Mediterranean coast, with ratio higher than Redfield
429 ratio (Markaki et al., 2010, Desboeufs et al., 2018). The highest ratio observed reached 1200 (in
430 case of DIN/TDP), but were on average around 100 in bulk deposition. The highest ratio could be
431 linked to a washout effect of the gaseous N species (as NO_x and NH_3) by rain (Ochoa-Hueso et al.,
432 2011). At the two stations, no high NO_x concentrations were observed in the boundary layer before
433 wet deposition. The presence of nitrate and ammonium in the background aerosols has been
434 emphasized during recent campaigns in the remote Mediterranean atmosphere (e.g. Mallet et al.,
435 2019). To our knowledge, no data are available on both P and N concentrations in Mediterranean
436 aerosols. The lowest concentrations of P relative to N in aerosol particles in Mediterranean have
437 been observed during the cruise (Fu et al., in prep.). The TDP concentrations were consistent with
438 the average value of 8.4 $\mu\text{g L}^{-1}$ measured in African dust rain samples collected in Spain over the
439 1996-2008 period (Izquierdo et al., 2012). Inorganic phosphorus predominated in the dust-rich rain,
440 whereas organic P was dominant in the background rain as the contribution of DOP to the TDP was
441 60% and 44% in Rain ION and Rain FAST, respectively. The DOP/TDP ratio presents a very large
442 range in Mediterranean rains, spanning from 6% in Spanish dusty rain samples (Izquierdo et al.,
443 2012) to 75-92% in rains from Crete Islands (Violaki et al., 2018). A reason for this wide range
444 could be that Mediterranean European aerosols, as opposed to Saharan dust particles, are dominated
445 by organic phosphorus compounds associated with bacteria (Longo et al., 2014).



446

447 **Figure 5: Comparison of dissolved (D) and total (T) TMs concentrations along with data from 14 former studies**
 448 **carried out in the eastern and western Mediterranean Sea.**

449 The dissolved and total TMs concentrations in the PEACETIME rains were lower than those
 450 reported in coastal areas (eastern Basin: Özsoy and Örnektekin, 2009; Al-Momani et al., 1998;
 451 Kanellopoulou et al, 2001 and western Basin: Guieu et al., 1997; Guerzoni et al., 1999b; Chester et
 452 al., 1997; Losno, 1989; Frau et al., 1996) (Fig. 5), notably for the background Rain ION. This
 453 suggests the probable effect of both local anthropogenic influence at coastal sites due to higher
 454 aerosol concentrations in comparison to remote Mediterranean (Fu et al., in prep.) and due to the
 455 reduction of anthropogenic emission for some elements since most of the referenced works on
 456 coastal rainwaters date from the late 1990s. This is particularly true for Cd and Pb whose emissions
 457 have strongly decreased over the last decades, notably due to removal of lead in gasoline and
 458 reduction of coal combustion (Pacyna et al., 2007). This has resulted in a clear decrease in the
 459 particulate concentrations of these metals in the Mediterranean atmosphere (Migon et al., 2008),



460 consistent with the fact that concentrations in the PEACETIME rains are one to two orders of
461 magnitude lower than reported in the literature. For these metals, the discrepancy is also observed
462 between the concentrations in our open-sea rain samples and the concentrations measured in three
463 rains collected at sea in April 1981 (Dulac, 1986), confirming the large decrease of concentrations
464 could be related with the decrease of emission. Thus, our results show the former literature cannot
465 be used as current reference about coastal rain composition due to recent environmental mitigation
466 on metals emissions.

467 4.1.2. Enrichment factor

468 EF and solubility values of TMs and P observed during the two rain events were very contrasted
469 (Fig. 6). In Rain ION, almost all elements were significantly enriched relative to earth crust (EF
470 >10 , and up to $\sim 10^3$ for Cd and Zn), whereas in Rain FAST, only Zn (73), Cd (48) and Mo (15)
471 were slightly enriched. Only Ti, Fe, and Mn did not present a significant enrichment (EF < 10) in
472 Rain ION, in agreement with previous studies in the Mediterranean environment showing that these
473 metals are mainly associated with mineral dust in atmospheric deposition (e.g., Guieu et al., 2010;
474 Desboeufs et al., 2018). Both rains, EF of Zn was in average five times higher than EF found in the
475 rains previously studied in the Mediterranean region (Özsoy and Örnektekin, 2009; Al-Momani et
476 al., 1998; Losno, 1989). However, extremely high enrichments of Zn in rainwater have also been
477 reported by Frau et al. (1996) with a geometric mean EF of about 6500 in both crust-rich and crust-
478 poor rains from two sites in southern Sardinia. Fu et al. (2017) also reported EF higher than 1000
479 for Zn in atmospheric bulk deposition in Lampedusa Island. The anthropogenic origin of particulate
480 TMs and P have been reported by several studies on atmospheric deposition in the western
481 Mediterranean (e.g., Guieu et al., 2010; Sandroni and Migon, 2002; Desboeufs et al., 2018). For
482 example, Desboeufs et al. (2018) showed that there is a large contribution of anthropogenic
483 combustion sources in P, Cr, V and Zn background deposition fluxes. Aerosol composition
484 monitoring over Mediterranean coastal area showed the role of land-based sources and ship traffic
485 sources on TMs contents (Bove et al., 2016; Becagli et al., 2017). However, all these sampling sites
486 were located in coastal areas, where it was difficult to discriminate the potential local influences.
487 Here, even if the on-board atmospheric gas and particle measurements did not show a specific
488 anthropogenic influence during the period of Rain ION, the particles scavenged by this rain
489 presented a clear anthropogenic signature for all TMs except Ti, Fe and Mn; however for Fe and
490 Mn, an influence of non-crustal sources in Rain ION is visible through a clear increase in the EF
491 values compared to FAST (Fig. 6). This means that even over remote Med Sea, the chemical



492 composition of background aerosol particles is likely continuously impacted by anthropogenic
493 sources.

494 Moreover, the EF values of TMs for Rain FAST were significantly lower than for Rain ION (Fig.
495 6) but similar to Saharan rains (Guerzoni et al., 1999b; Özsoy and Örnektekin, 2009). The
496 comparison between dust-rich and background rains generally reveals a net difference of
497 concentrations (at least higher by a factor 3 in dust-rich), notably for Al, Fe, Mn and Cr (Guerzoni
498 et al., 1999b; Özsoy and Örnektekin, 2009). Such contrast was indeed observed for Al, Fe and Mn
499 in the PEACETIME rains (Fig. 5), but also for Cu and Pb. The combination of higher concentrations
500 and EF values <10 found in Rain FAST confirm that the dust contribution was important on
501 deposition fluxes of many TMs.

502 4.1.3. Solubility

503 The solubility values were also larger in Rain ION than in the dusty Rain FAST, except for Mo for
504 which the difference between both rain samples is not significant (Fig. 6). For Rain ION, TMs and
505 P presented solubility higher than 78%, except for Cr (38%). In Rain FAST, solubility values <10%
506 were observed for Al and Fe, more than 10 times lower than in Rain ION. For the other TMs, the
507 highest difference in solubility was observed for Pb whose solubility decreased from 97% in Rain
508 ION to 27% in Rain FAST. In a review on TMs solubility in Mediterranean rainwaters collected in
509 coastal areas, Desboeufs (2021) emphasize the large range of solubility for all the TMs: Fe (0.8-
510 41%), Cr (6-80%), Pb (5-90%), Ni (22-93%), Mn (16-95%), Cu (22-96%), Zn (14-99%), V (35-
511 99%) and Cd (72-99%). The solubility ranges found in this study were generally consistent with
512 those reviewed by Desboeufs (2021). In particular, the Mn solubility values in FAST (60%) and
513 ION (92%) rains are close to those reported by Dulac (1986) from a dust-rich (57%) and an
514 anthropogenic (83%) rain collected at sea in the Ligurian Sea and west of Sardinia in April 1981,
515 respectively. Only Fe solubility (84%) found in Rain ION was higher than the average values
516 previously reported. In the Rain FAST, Fe solubility was 8%, this is 10 times lower than average
517 Fe solubility in 10 dust-rich rains collected on the southeastern coast of Sardinia by Guerzoni et al.
518 (1999b), but consistent with Saharan dust wet deposition collected in the Atlantic Ocean (Chance
519 et al. 2015; Powell et al., 2015; Baker et al., 2017).



520

521 **Figure 6: Enrichment Factors (EF, upper panel) and solubility (% ,bottom panel) of phosphorus (P) and TMs**
522 **ordered by increasing EF in the two rainwater samples.**

523 Few studies compared TMs solubility between dust-rich and background rains in the Mediterranean.
524 In Sardinia, Guerzoni et al. (1999b) observed an increase in solubility values from dust-rich to
525 background rains for Al, Cr, Fe and Pb (and hardly for Cd), and reported an inverse relationship
526 between the particle concentration and solubility of Al, Fe, Pb and Cd. Similarly, Theodosi et al.
527 (2010) showed a decrease in TMs solubility with the increase in dust load in rains collected on Crete
528 Island. In those two studies, this decrease was dependent on the considered metal, with Pb
529 presenting the highest decrease in solubility. The decrease in solubility from background to dust-
530 rich rains was also observed for P in Spain by Izquierdo et al. (2012), with values of solubility
531 decreasing from 25% to 7%, and for Mn in offshore rains as mentioned above (Dulac, 1986). Metal
532 partitioning in rainwater can be influenced by a number of parameters, such as pH, presence of
533 dissolved organic complexing ligands, in-cloud processes, particle origin and load (Desboeufs et
534 al., 1999; Bonnet and Guieu, 2004; Paris and Desboeufs, 2013; Heimburger et al., 2013). However,
535 the particulate desert dust load, reflecting dust vs anthropogenic signature, is the main control of
536 TMs solubility in the Mediterranean rainwater (Özsoy and Örnektekin, 2009; Theodosi et al., 2010).
537 A much lower solubility of TMs in Rain FAST than in Rain ION (except for Mo) is consistent with



538 the EFs in Rain FAST (Fig. 6), although no correlation between solubility and EF values could be
539 observed. The case of Mo is unique, since its solubility was comparable in Rains ION and FAST
540 despite a >20 times higher EF in Rain ION. As Mo solubility is seldom studied in the literature, we
541 could not conclude on the reason for this particular outcome. It is interesting to note that despite the
542 desert signature, the majority of metals have solubility greater than 50% in rain FAST.

543 **4.2. Atmospheric wet deposition as a source of TMs to the surface seawater**

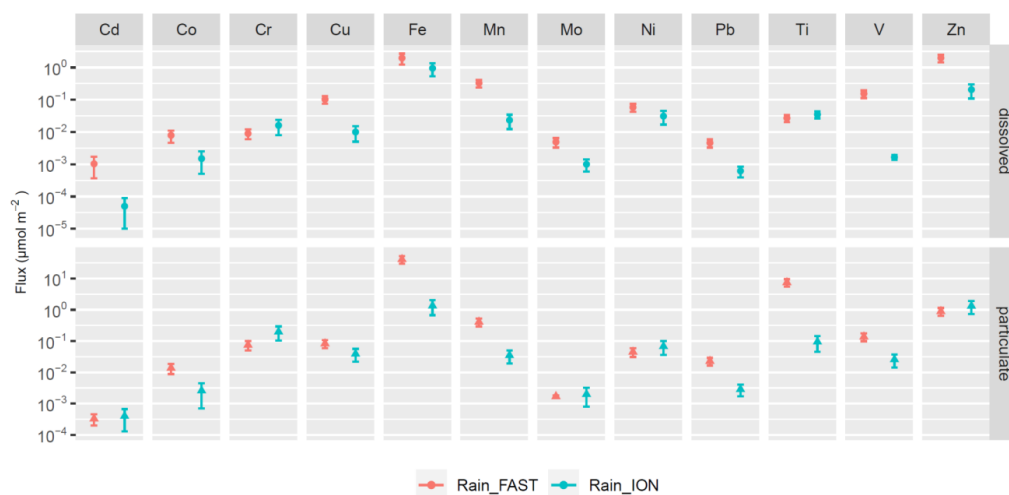
544 *4.2.1. Atmospheric fluxes*

545 As mentioned before, the two collected rains were part of large rain systems, associated with patchy
546 rainfalls that lasted several hours or days (section 3.1). This spatio-temporal variability led to
547 heterogeneity in both rainwater concentrations and accumulated precipitation across the studied
548 region. Such spatial variability has been observed by Chance et al. (2015) in the Atlantic Ocean.
549 Moreover, even weak lateral advection can transfer surface water impacted by intense precipitation
550 in the vicinity of the vessel. On this basis, the spatial extrapolation of wet deposition fluxes seems
551 subject to a large uncertainty when the rain samples are not collected across the rain area (Chance
552 et al., 2015). To best counteract this effect, spatial variability was taken into account to quantify the
553 total precipitation i.e. 3.5 ± 1.2 mm for rain ION and 6.0 ± 1.5 mm for rain FAST (see 3.1) in order
554 to quantify the wet deposition fluxes.

555 From the total (dissolved + particulate) Al concentration measured in the rain FAST sample, we
556 estimated the wet mineral dust deposition flux at 65 ± 18 mg m⁻², assuming 7.1% Al in dust (Guiou
557 et al., 2002). The vertical distribution of dust particles (Fig. 2b) and the absence of high Al
558 concentrations close to the sea surface (Fu et al., in prep.) indicate that dust dry deposition can be
559 neglected. Based on the increase in total Al in the upper 20 m of the column water following the
560 deposition events, Bressac et al. (2021) derived an average dust deposition flux of ~ 55 mg m⁻² at
561 FAST station, comparable to our estimate. Although low compared to deposition fluxes reported in
562 the western Mediterranean (Bergametti et al., 1989; Loje-Pilot and Martin, 1996; Ternon et al.,
563 2010), such flux values are among the most intense weekly dust deposition fluxes recorded more
564 recently in Corsica between 2011 and 2013 and is equivalent to the mean weekly flux observed in
565 Majorca Island during the same period (Vincent et al., 2016). The aerosol columnar during the dust
566 event being estimated between 0.18 and 0.24 g m⁻² (see 3.1.), the expected maximum values of
567 atmospheric dust flux could be in this range. The comparison with the estimated flux indicates that
568 the atmospheric column was probably not totally washed-out by the short rain event. Indeed, Fig.
569 2b shows that a significant depolarization was observed immediately after the rain ended on the



570 ship, before atmospheric advection could have brought dusty air possibly not affected by rain.
571 Satellite products (Fig. S2) confirm that on 5 June, the dusty air mass was transported farther to the
572 north-east from the station where it was replaced by clear air.



573

574 **Figure 7: Dissolved (upper panels) and particulate (lower panels) wet deposition fluxes ($\mu\text{mol m}^{-2}$) for**
575 **the different TMs estimated from the two rains sampled on board, considering the standard deviation**
576 **on the TMs concentrations and the spatial variability of total precipitation over the area of sampling**
577 **(Rain ION in blue and Rain FAST in red).**

578 The atmospheric dissolved and particulate wet deposition fluxes of TMs, derived from the chemical
579 composition of rain samples and total precipitation, are presented in Fig. 7. Co, Mo and Cd
580 presented the lowest fluxes in the two rainfalls. Zn and Fe fluxes were in the same order of
581 magnitude and were the highest dissolved fluxes compared to the other TMs in the two rains. The
582 comparison showed that almost all the dissolved TMs fluxes were higher in the dusty rain, except
583 Cr and Ti. For the particulate phase, the fluxes were mainly increased by dust deposition for Co,
584 Fe, Mn, Pb, Ti and V. Our results emphasized that dust deposition, even here in case of a moderate
585 deposition flux, enabled higher atmospheric inputs of TMs than a low perturbed-anthropogenic
586 background rain. This is notably the case for dissolved Cd, Cu, Mn, V and Zn and for particulate
587 Fe and Ti with more than one order of magnitude fluxes difference between the two rains. The
588 orders of magnitude found in this study could be used as “typical atmospheric fluxes” to estimate
589 atmospheric inputs of TMs by a rain event to the western Med Sea. We must keep in mind, however,
590 that annual and long-term deposition fluxes of dust-related elements (e.g. TERNON et al., 2010), but



591 also nitrogen (e.g., Richon et al., 2018b), in the Med Sea, are dominated by a few atypical intense
592 deposition events when they occurred.

593 4.2.2. Comparison between TMs wet deposition inputs and marine stocks at ION and FAST stations

594 Marine sampling sequences carried out before and after rains were, to our knowledge, the first direct
595 observations to trace the fate of atmospheric metals and nutrients in the water column after wet
596 deposition event. The time chart of the sampling of rain and column water (surface microlayer,
597 subsurface seawater and mixed layer) is presented in Fig. 8. The impact of the two wet depositions
598 on nutrients stocks in the Mediterranean surface waters is discussed in van Wanbeke et al. (2020)
599 and Pulido-Villena et al. (2021). Both nitrate and DIP increased in the ML following the rains.
600 Although the closure of the N and P budgets had to take into account post-deposition processes as
601 new nutrient transfer through the microbial food web (uptake, remineralisation, and
602 adsorption/desorption processes on sinking particles), it was shown that wet deposition was a
603 significant source of nutrients for ML during the cruise. We focus here on the role of TMs deposition
604 as a source of metals to the column water. To do so, we estimated the potential enrichment of SML
605 and ML from the rain by calculating the difference (Δ) in TMs stocks before and after rains.



606
607 **Figure 8: Sampling chronology during the ION and FAST stations for SML, SSW and ML. The blue**
608 **periods correspond to rainfall in the station area (after ERA 5 reanalysis and radar imagery, see**
609 **section 3.1). Samplings were performed 4 days and 2 days before and 2 h after Rain ION, and at a**
610 **higher frequency at the FAST station: 57, 37 and 7.5 hours before and 4.5, 12, 24 hours after Rain**
611 **FAST. SML and SSW samples could not be collected immediately before and after the rains because**
612 **of bad weather conditions, and were collected 3 and 4 days before Rain ION, and 57 and 20 h before**
613 **and 30 h after Rain FAST.**

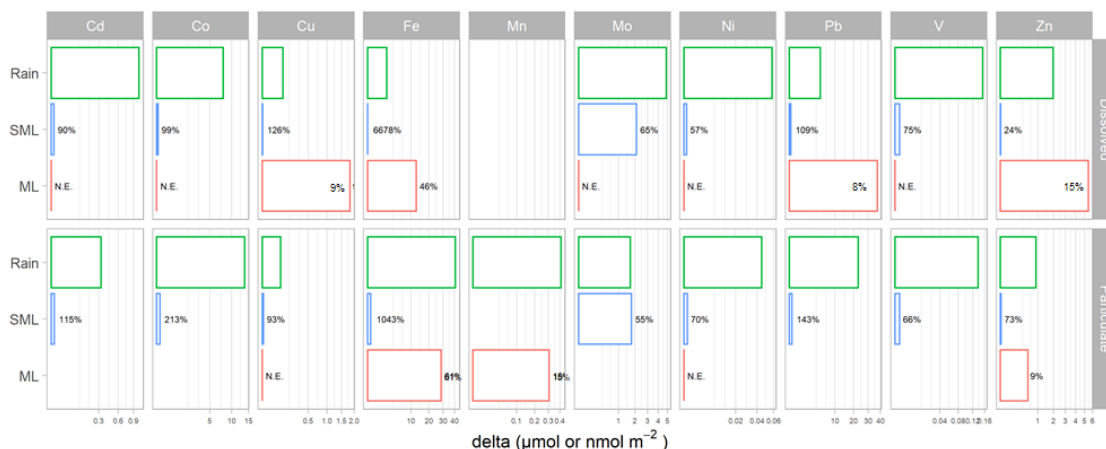
614 At ION, no SML sampling was done after rain, preventing the study of the rain effect. For ML, the
615 large variability in total and dissolved stocks between the two casts ML25 and ML27 before the
616 rain makes the establishment of a background concentration levels before rain difficult. ML27 was
617 used as initial conditions since it is the closest sampling from post-rain measurements (ML29). As



618 mentioned previously, dust rain deposition over the FAST station area started on 3 June. Bressac et
619 al. (2021) showed that the dust signature, traced by changes in Al and Fe stocks in the ML, was
620 already visible from the ML03 sampling. We defined the enrichment of seawater layers as the
621 difference between the maximum stocks after rains (from SML 04 or 06 and ML05+4) and the
622 initial seawater stocks (SML02 and ML02).

623 At ION, only particulate Cu (+27%) and Zn (+44%) stocks increased in the ML after the rain. Even
624 if the dissolved forms of Cu and Zn predominated in the ML, this increase was accompanied by
625 increasing K_d values, i.e. in the particulate/dissolved partitioning (0.07 vs 0.12 for Cu and 0.14 vs
626 0.2 for Zn). This was also the case for Fe (K_d increased from 2.6 to 4.3), although no significant
627 difference (<5%) was observed on the particulate Fe stock. The K_d values in the ION rain sample
628 being higher than in the marine stock before the rain, that suggests the wet deposition at ION is
629 mainly an additional source of particulate TMs.

630 At FAST, the ML stocks increased in the particulate phase for Fe (+61%), Mn (+15%) and Zn
631 (+9%) and in the dissolved phase for Cu (+9%), Fe (+46%), Pb (+8%) and Zn (+15%) (Fig. 9). In
632 addition of marine inventories, the particulate TMs input by rain was also observed on K_d values
633 and total X/Al in the ML. For example, $K_d(\text{Fe})$ increased from 0.14 to 0.17 in ML and its K_d was
634 0.25 in the rain. Even for Ni for which no change in stock could be evidenced, $K_d(\text{Ni})$ decreased
635 from 0.1 to 0.07 and its K_d in the rain was 0.006. For Mn/Al which fell from 0.27 before the rain to
636 0.008 after the rain (ML05+4), in accordance with the rain ratio (0.004). In the SML, the dissolved
637 and particulate stocks increased following rains for all TMs, from a factor 1.5 (Mo) to 10 (Fe) for
638 the dissolved phase and from a factor 1.6 (Ni) to 67 (Fe) for the particulate phase (Fig. 9).





640 **Figure 9: Comparison between TMs wet deposition fluxes (in green) and TMs marine stock delta**
641 **(before and after the rain) in the SML (in blue) and in the ML (in red) at FAST. Dissolved = upper**
642 **panels and particulate = lower panels. Marine stocks increase are expressed in absolute values (Cd,**
643 **Co and Pb stocks in nmol m^{-2} , and the other TMs in $\mu\text{mol m}^{-2}$) and in relative values (%). N.E.: not**
644 **enhanced (increase <5%).**

645 The comparison between the observed enhancements in the SML stocks and the rain inputs at FAST
646 (Fig. 9) indicates that the atmospheric fluxes support all observed deltas. Indeed, the atmospheric
647 particulate and dissolved fluxes of TMs were 2 to 4 orders of magnitude higher than the mean stocks
648 present in the SML, except Mo which was in the same order of magnitude. In the ML, the magnitude
649 of atmospheric particulate inputs was higher or similar to the particulate marine delta of Fe, Mn and
650 Zn. For Cu, Fe, Pb and Zn, the increase in dissolved stocks within the ML was 2 to 10 times higher
651 than what could provide the atmospheric inputs. As described in Guieu et al. (2020), marine
652 dynamical conditions at FAST were favorable to observe any change in the water masses strictly
653 attributed to external inputs coming from the atmosphere on a short time scale. However, a
654 cumulative effect of previous and surrounding wet deposition events could explain this difference
655 between atmospheric inputs from rain FAST and increase of marine dissolved stocks. We cannot
656 exclude the possibility of lateral transport of metals from surrounding waters being enriched by the
657 rain events of June 3 for example, as revealed by the increase in the 0-20 m Fe and Al inventories
658 (Bressac et al., 2021). Another hypothesis to explain that higher stock increases of metals in the ML
659 than the one derived from atmospheric deposition is related to post-deposition processes. Indeed,
660 once deposited, the atmospheric particulate fraction could still be partly solubilized in seawater, as
661 the solubilisation of TMs (e.g. Fe) could occur over several hours or days (Wagener et al., 2008;
662 Wuttig et al., 2013; Desboeufs et al., 2014). This could lead to an underestimate of dissolved TMs
663 atmospheric inputs. Moreover, the time lag between the rain and the first SML sampling (1 day)
664 does not allow us to conclude on the role played by SML as a “trap” of the added dissolved metals
665 by rain. However, results showed clearly the increase of dissolved TMs in the SML even 24 h after
666 the rain (Fig. 9). Even if this increase could be due to dissolution processes (Tovar-Sanchez et al.,
667 2020), we cannot exclude that the residence time of dissolved atmospheric TMs in the SML was
668 sufficient to mask the atmospheric inputs in the ML05+4 sample. It is also known that dissolved
669 concentrations in the ML are subject to various biological processes such as phytoplankton uptake
670 (Morel et al., 2003). The comparison between ML05+4 and ML05+12 samples performed after the
671 rain shows that the dissolved and particulate stocks decreased quickly for all the TMs (not shown),
672 in agreement with the predominance of removal processes (sedimentation, biological transfer,
673 adsorption) on these stocks. However, the rate of decrease depended on the TMs, showing that some



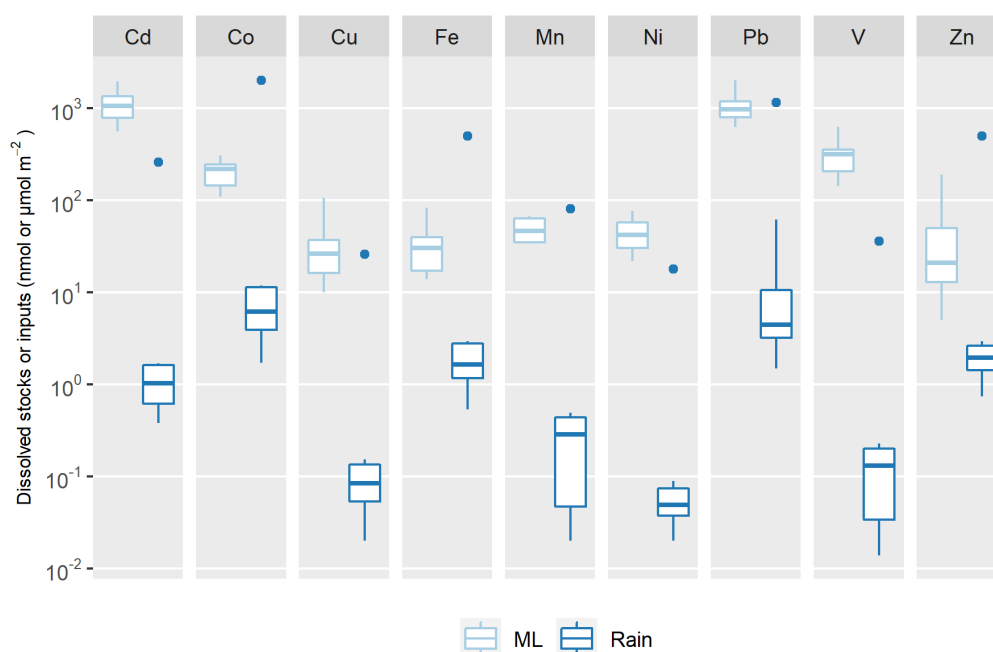
674 removal processes predominate over others depending on the metal. For example, the dissolved
675 metals decrease could correspond to scavenging onto particles, which is a common physical-
676 chemical process occurring in the ocean for Fe (Wagener et al., 2010; Bressac and Guieu., 2013) or
677 Co (Migon et al., 2020). Finally, our results show that dust wet deposition was a net source of all
678 the studied trace metals for SML both in the dissolved and particulate fraction. For ML, atmospheric
679 dust inputs were also a net source of particulate Fe, Mn, and Zn, and dissolved Cu, Fe, Pb and Zn.
680 Due to various marine post-deposition processes, it was more complicated to observe the effect of
681 wet deposition on dissolved stocks, explaining why the SML and ML particulate stocks were more
682 impacted by rain than the dissolved stocks. On a timescale of hours, Fe inventory was the most
683 impacted by the dusty rain input, both in dissolved and particulate phase, confirming that the dust-
684 rich rains are a net source of Fe to the surface Mediterranean Sea (Bonnet and Guieu, 2006, Bressac
685 et al., 2021).

686 *4.2.3. Comparison between TMs wet atmospheric inputs and marine stocks at the scale Western* 687 *and Central Mediterranean Sea*

688 As observed from dissolved TMs stocks measured before and after the rains, a large part of
689 uncertainties in the data analysis results from various removal processes of TMs after wet
690 deposition, which could have time resolution shorter than the sampling step. In order to limit the
691 effect on these potential processes in data analysis, here we further study the role of wet deposition
692 by comparing atmospheric dissolved fluxes to marine dissolved stocks by using TMs profiles in the
693 ML at all 13 marine stations, i.e. 22 ML samplings, throughout the whole cruise (Fig. 10). Indeed,
694 considering that the collected rains were originating from large rain systems covering more than
695 50 000 km² around the sampling zone and were typical of Mediterranean wet deposition, we
696 hypothesized that they could have occurred in any of the explored areas during the cruise.
697 Exceptional intense dust deposition events have been recorded in the Mediterranean, reaching 20 g
698 m⁻² (Bonnet et al., 2006). Sporadic and intense wet dust deposition higher than 1 g m⁻² are regularly
699 observed in the spring in the western Mediterranean basin (e.g., Vincent et al., 2016). At the
700 beginning of the cruise, an intense wet dust deposition event (not collected) occurred over the South
701 of Sardinia and over the Tyrrhenian Sea with fluxes reaching about 9 g m⁻² (Bressac et al., 2021).
702 In order to take into account the effect of such an event, we also estimated the atmospheric fluxes
703 of dissolved metals based on a 9 g m⁻² wet dust deposition event considering solubility values found
704 in the rain FAST (Fig. 10). The metal solubility decreasing with increasing dust load (Theodosi et
705 al., 2010), this estimation constitutes probably a maximum value of the dissolved inputs of trace
706 metals by such a dust deposition event. In addition to removal processes, the impact of rain inputs



707 on TMs marine stocks is also controlled by MLD fluctuations that we ignored in the work described
708 above by using a fixed depth for FAST an ION stations. However, the variability of this MLD (7-
709 21 m during the cruise, typical of Med thermal stratified period) could change the marine budgets
710 by a factor of 3. So we considered the measured MLD (Van Wambeke et al., 2020) for calculating
711 marine budgets of TMs at each station.



712

713 **Figure 10: Comparison of marine stocks in the ML at all the stations occupied during the**
714 **PEACETIME cruise with atmospheric inputs estimated (1) from ION and FAST rains (Boxes) and (2)**
715 **from an intense wet dust deposition event of 9 g m^{-2} (blue dots). Cd, Co and Pb stocks are in nmol m^{-2} ,**
716 **and the other TMs in $\mu\text{mol m}^{-2}$. For Mn, marine stocks are derived from surface concentrations close**
717 **to Corsica coasts (Wuttig et al., 2013: samples OUT at 0, 5 and 10 m) and in the Ionian Sea (Saager et**
718 **al., 1993: Bannock basin at 0, 10, and 15 m), as no measurement is available from the PEACETIME**
719 **cruise. Boxes and whiskers as in Fig. 4.**

720 Applying to the whole transect, the atmospheric inputs, obtained from our rain composition, were
721 at least 100-fold smaller than the dissolved stocks in the mixed layer, except for Co, Fe and Zn. The
722 atmospheric inputs represented more than 30% of the dissolved Zn stocks and 10 to 18% for Fe.
723 This significant input of dissolved Fe is in agreement with our field observations in the ML. For
724 Co, the maximum atmospheric fluxes estimated during the cruise represented >10% of stocks. Here



725 the comparison is based only on dissolved TMs in rain water, yet as discussed previously, the
726 solubilisation post-deposition of atmospheric particles in the water column could further enrich the
727 marine dissolved stocks. In the case of the intense dust deposition event, the dissolved inputs are of
728 the same order of magnitude as marine stocks for Co, Fe, Mn, Pb and Zn. The enrichment in
729 dissolved Fe and Mn was previously observed by Wuttig et al. (2013) after artificial dust seeding
730 in large mesocosms (simulating a wet deposition event of 10 g m^{-2}). The surface seawater could be
731 significantly affected by the deposition of these dissolved elements in the case of wet dust
732 deposition. The marine TMs concentrations measured during the cruise being typical of
733 Mediterranean surface seawater concentrations, we conclude from these comparisons that wet
734 deposition events, notably wet dust deposition events, prove to be an external source of dissolved
735 TMs for the Mediterranean Sea during the period of thermal stratification.

736 5. Conclusions

737 This study provides both the dynamical properties and chemical characterization of two rainwaters
738 collected in the open Mediterranean Sea, concurrently with TMs marine stocks in surface seawater.
739 Our results are the only recent report of concentrations, EF and solubility values for TMs in rain
740 samples collected in remote Med Sea. By highlighting the discrepancy between TMs concentrations
741 with the previous and coastal rain studies, this work demonstrates the need to provide a new and
742 recent database on metal composition in Mediterranean rains in order to estimate the role of
743 atmospheric TMs deposition. We showed the representativeness of rain FAST as typical Saharan
744 dust wet deposition as well in its chemical composition as in its magnitude and extent, whereas Rain
745 ION is a typical low perturbed anthropogenic background rain of remote Med Sea. On this basis,
746 we suggest to use the chemical composition of PEACETIME rains as a new reference for the studies
747 of TMs on wet deposition in Med Sea.

748 Since atmospheric TMs have been identified as critical oligo-nutrients for marine biosphere, our
749 study is the first *in situ* evidence that atmospheric wet deposition constitutes a significant external
750 source for some of these elements to surface stratified Mediterranean seawater. Our results show
751 that the original approach developed here is very relevant in this purpose and could be used in other
752 part of the world where atmospheric deposition is suspected to impact marine biosphere, as HNLC
753 areas.

754

755



756 **Data availability.** Guieu et al., Biogeochemical dataset collected during the PEACETIME cruise. SEANOE.
757 <https://doi.org/10.17882/75747> (2020). Atmospheric Data are accessible on <http://www.obs->
758 [vlfr.fr/proof/php/PEACETIME/peacetime.php](http://www.obs-vlfr.fr/proof/php/PEACETIME/peacetime.php).

759 **Author contributions.** KD and FF designed the study and wrote the manuscript; FF, ST, JFD, Ch.G made
760 the on-board atmospheric measurements and sampling during the cruise; FF, ST and JD analysed the rain
761 samples; MB, ATS, and ARR made the marine TMs sampling and analyses; PF was the reference scientist
762 of PEGASUS, AF and FM managed all the technical preparation of atmospheric samplings, PC analysed the
763 lidar data; KD, FD and Ce.G designed the cruise strategy; KD and Ce.G coordinated the PEACETIME
764 project, FD coordinated the ChArMEx funding request, and near-real time and forecast survey of
765 atmospheric conditions during the cruise; all the authors commented on the manuscript and contributed to
766 its improvement.

767 **Competing interests.** The authors declare that they have no conflict of interest.

768 **Special issue statement.** This article is part of the special issue “Atmospheric deposition in the low-nutrient–
769 low-chlorophyll (LNLC) ocean: effects on marine life today and in the future (ACP/BG inter- journal SI)”.
770 It is not associated with a conference.

771 **Acknowledgements.** The authors wish to thank Thierry Alix the captain of the R/V *Pourquoi Pas ?* as well
772 as the whole crew and technical staff for their involvement in the scientific operation. We gratefully thank
773 Thibaut Wagener for his involvement in the trace-metals clean marine sampling and Mickaël Tharaud for
774 the HR-ICP-MS analysis. We thank the Leosphere Technical support team and especially Alexandre Menard
775 for their remote assistance with LIDAR repair under difficult off-shore conditions. H el ene Ferr e and the
776 AERIS/SEDOO service are acknowledged for real-time collection during the cruise of maps from
777 operational satellites and forecast models used in this study, with appreciated contributions of EUMETSAT
778 and AERIS/ICARE for MSG/SEVIRI products. EUMETNET is acknowledged for providing the pan-
779 European weather radar composite images through its OPERA programme. We acknowledge the US
780 National Oceanic and Atmospheric Administration (NOAA) Air Resources Laboratory (ARL) for the
781 provision of the HYSPLIT (HYbrid Single-Particle Lagrangian Integrated Trajectory) model via NOAA
782 ARL READY website (<http://ready.arl.noaa.gov>) used in this publication. This study is a contribution to
783 the PEACETIME project (<http://peacetime-project.org>; last accessed 05/04/2021), a joint initiative of the
784 MERMEX and ChArMEx programmes supported by CNRS-INSU, IFREMER, CEA and M et eo-France as
785 part of the decadal meta-programme MISTRALS coordinated by CNRS-INSU. PEACETIME was endorsed
786 as a process study by GEOTRACES and is also a contribution to IMBER and SOLAS international programs.

787

788 References

789 Achterberg, E. P., Braungardt, C. B., Sandford, R. C. and Worsfold, P. J.: UV digestion of seawater samples prior to
790 the determination of copper using flow injection with chemiluminescence detection, *Anal. Chim. Acta*, 440, 27–36,
791 [https://doi.org/10.1016/S0003-2670\(01\)00824-8](https://doi.org/10.1016/S0003-2670(01)00824-8), 2001.

792 Al-Momani, I. F., Aygun, S., and Tuncel, G.: Wet Deposition of Major Ions and TMs in the Eastern Mediterranean
793 Basin, *J. Geophys. Res. (Atmos.)*, 103, 8287–8299, <https://doi.org/10.1029/97JD03130>, 1998.



- 794 Amato, F., Alastuey, A., Karanasiou, A., Lucarelli, F., Nava, S., Calzolari, G., Severi, M., Becagli, S., Gianelle, V. L.,
795 Colombi, C., Alves, C., Custódio, D., Nunes, T., Cerqueira, M., Pio, C., Eleftheriadis, K., Diapouli, E., Reche, C.,
796 Minguillón, M. C., Manoussakos, M.-I., Maggos, T., Vratolis, S., Harrison, R. M., and Querol, X.: AIRUSE-LIFE+: a
797 harmonized PM speciation and source apportionment in five southern European cities, *Atmos. Chem. Phys.*, 16, 3289–
798 3309, <https://doi.org/10.5194/acp-16-3289-2016>, 2016.
- 799 Annett, A. L., Lapi, S., Ruth, T. J., and Maldonado, M. T.: The effects of Cu and Fe availability on the growth and Cu:C
800 ratios of marine diatoms, *Limnol. Oceanogr.*, 53, 2451–2461, <https://doi.org/10.4319/lo.2008.53.6.2451>, 2008.
- 801 Avila, A., Queralt - Mitjans, I., and Alarcón, M.: Mineralogical composition of African dust delivered by red rains over
802 northeastern Spain, *J. Geophys. Res. Atmos.*, 102, 21977–21996, <https://doi.org/10.1029/97JD00485>, 1997.
- 803 Bacconnais, I., Rouxel, O., Dulaquais, G., and Boye, M.: Determination of the copper isotope composition of seawater
804 revisited: A case study from the Mediterranean Sea, *Chem. Geol.*, 511, 465–480,
805 <https://doi.org/10.1016/j.chemgeo.2018.09.009>, 2019.
- 806 Baker, A. R., and Jickells, T. D.: Atmospheric deposition of soluble trace elements along the Atlantic Meridional
807 Transect (AMT), *Prog. Oceanogr.*, 158, 41–51, <https://doi.org/10.1016/j.pocean.2016.10.002>, 2017.
- 808 Becagli, S., Anello, F., Bommarito, C., Cassola, F., Calzolari, G., Iorio, T. D., Sarra, A. D., Gómez-Amo, J. L., Lucarelli,
809 F., Marconi, M., and Meloni, D.: Constraining the ship contribution to the aerosol of the central Mediterranean, *Atmosp.*
810 *Chem. Phys.*, 17, 2067–2084, , <https://doi.org/10.5194/acp-17-2067-2017>, 2017.
- 811 Bergametti, G., Gomes, L., Remoudaki, E., Desbois, M., Martin, D., and Buat-Ménard, P.: Present transport and
812 deposition patterns of African dusts to the North-Western Mediterranean, in *Paleoclimatology and Paleometeorology:*
813 *Modern and past patterns of global atmospheric transport*, Leinen, M., and Sarnthein, M., Eds., Springer, Dordrecht,
814 NATO ASI Ser. C, 282, 227–252, https://doi.org/10.1007/978-94-009-0995-3_9, 1989.
- 815 Béthoux, J.P., Courau, P., Nicolas, E., and Ruiz-Pino, D.: Trace metal pollution in the Mediterranean Sea, *Oceanol.*
816 *Acta* 13, 481–488, <https://archimer.ifremer.fr/doc/00103/21418/> (last accessed 03 July 2021), 1990.
- 817 Bonnet, S. and Guieu, C.: Dissolution of atmospheric iron in seawater, *Geophys. Res. Lett.*, 31, L03303,
818 <https://doi.org/10.1029/2003GL018423>, 2004.
- 819 Bonnet, S., and Guieu, C.: Atmospheric forcing on the annual iron cycle in the western Mediterranean Sea: A 1-year
820 survey, *J. Geophys. Res.*, 111, C09010, <https://doi.org/10.1029/2005JC003213>, 2006.
- 821 Bove, M. C., Brotto, P., Calzolari, G., Cassola, F., Cavalli, F., Fermo, P., Hjorth, J., Massabò, D., Nava, S., Piazzalunga,
822 A., and Schembari, C.: PM₁₀ source apportionment applying PMF and chemical tracer analysis to ship-borne
823 measurements in the Western Mediterranean, *Atmos. Environ.*, 125, 140–151,
824 <https://doi.org/10.1016/j.atmosenv.2015.11.009>, 2016.
- 825 Bressac, M., and Guieu, C.: Post-depositional processes: What really happens to new atmospheric iron in the ocean's
826 surface?, *Global Biogeochem. Cycles*, 27, 859– 870, doi:10.1002/gbc.20076, 2013
- 827 Bressac, M., Wagener, T., Leblond, N., Tovar-Sánchez, A., Ridame, C., Albani, S., Guasco, S., Dufour, A., Jacquet, S.,
828 Dulac, F., Desboeufs, K., and Guieu, C.: Subsurface iron accumulation and rapid aluminium removal in the
829 Mediterranean following African dust deposition, *Biogeosciences Discuss.*, <https://doi.org/10.5194/bg-2021-87>, in
830 review, 2021.
- 831 Bruland, K. W., Franks, R. P., Knauer, G. A. and Martin, J. H.: Sampling and analytical methods for the determination
832 of copper, cadmium, zinc, and nickel at the nanogram per liter level in sea water, *Anal. Chim. Acta*, 105, 233–245,
833 [https://doi.org/10.1016/S0003-2670\(01\)83754-5](https://doi.org/10.1016/S0003-2670(01)83754-5), 1979.
- 834 Buat-Ménard, P., and Chesselet, R.: Variable influence of the atmospheric flux on the trace metal chemistry of oceanic
835 suspended matter, *Earth Planet. Sci. Lett.*, 42, 399–411, [https://doi.org/10.1016/0012-821X\(79\)90049-9](https://doi.org/10.1016/0012-821X(79)90049-9), 1979.



- 836 Buat-Ménard, P.: Particle geochemistry in the atmosphere and oceans, In: Air-Sea Exchange of Gases and Particles,
837 Liss P.S., Slinn W.G.N. Editors, NATO ASI Series C, 108, 455–532, Springer, Dordrecht, https://doi.org/10.1007/978-94-009-7169-1_8, 1983..
- 839 Chance, R., Jickells, T. D. and Baker, A.R.: Atmospheric Trace Metal Concentrations, Solubility and Deposition Fluxes
840 in Remote Marine Air over the South-East Atlantic, *Mar. Chem.*, 177, 45–56,
841 <https://doi.org/10.1016/j.marchem.2015.06.028>, 2015.
- 842 Chazette, P., Flamant, C., Totems, J., Gaetani, M., Smith, G., Baron, A., Landsheere, X., Desboeufs, K., Doussin, J.-
843 F., and Formenti, P.: Evidence of the complexity of aerosol transport in the lower troposphere on the Namibian coast
844 during AEROCLO-sA, *Atmos. Chem. Phys.*, 19, 14979–15005, <https://doi.org/10.5194/acp-19-14979-2019>, 2019.
- 845 Chazette, P., Totems, J., Ancellet, G., Pelon, J., and Sicard, M.: Temporal consistency of lidar observations during
846 aerosol transport events in the framework of the ChArMEx/ADRIMED campaign at Minorca in June 2013, *Atmos.*
847 *Chem. Phys.*, 16, 2863–2875, <https://doi.org/10.5194/acp-16-2863-2016>, 2016.
- 848 Chester, R., Nimmo, M., Corcoran, P. A.: Rain water-aerosol trace metal relationships at Cap Ferrat: a coastal site in
849 the Western Mediterranean, *Mar. Chem.*, 58, 293–312, [https://doi.org/10.1016/S0304-4203\(97\)00056-X](https://doi.org/10.1016/S0304-4203(97)00056-X), 1997.
- 850 Desboeufs, K., Losno, R., Vimeux, F., Cholbi, S.: the pH-dependent dissolution of wind transported Saharan dust. *J.*
851 *Geophys. Res.*, 104, 21287–21299, <https://doi.org/10.1029/1999JD900236>, 1999.
- 852 Desboeufs, K., Leblond, N., Wagener, T., Bon Nguyen, E., Guieu, C.: Chemical fate and settling of mineral dust in
853 surface seawater after atmospheric deposition observed from dust seeding experiments in large mesocosms,
854 *Biogeosciences*, 11, 5581–5594, <https://doi.org/10.5194/bg-11-5581-2014>, 2014.
- 855 Desboeufs, K., Bon Nguyen, E., Chevaillier, S., Triquet, S., and Dulac, F.: Fluxes and sources of nutrient and trace
856 metal atmospheric deposition in the northwestern Mediterranean, *Atmos. Chem. Phys.*, 18, 14477–14492,
857 <https://doi.org/10.5194/acp-18-14477-2018>, 2018.
- 858 Desboeufs, K.: Trace metals and contaminants deposition, in *Atmospheric Chemistry in the Mediterranean – Vol. 2,*
859 *From Pollutant Sources to Impacts*, edited by Dulac, F., Sauvage, S., and Hamonou, E., Springer, Cham, Switzerland,
860 in press, 2021.
- 861 Dulac, F.: Dynamique du transport et des retombées d’aérosols métalliques en Méditerranée occidentale, PhD
862 Dissertation, Univ. Paris 7, 241 pp., 1986.
- 863 Formenti, P., D’Anna, B., Flamant, C., Mallet, M., Piketh, S. J., Schepanski, K., Waquet, F., Auriol, F., Brogniez, G.,
864 Burnet, F., Chaboureaud, J., Chauvigné, A., Chazette, P., Denjean, C., Desboeufs, K., Doussin, J., Elguindi, N.,
865 Feuerstein, S., Gaetani, M., Giorio, C., Klopper, D., Mallet, M. D., Nabat, P., Monod, A., Solmon, F., Namwoonde, A.,
866 Chikwililwa, C., Mushi, R., Welton, E. J., and Holben, B.: The Aerosols, Radiation and Clouds in southern Africa field
867 campaign in Namibia: Overview, illustrative observations, and way forward, *Bull. Am.Meteorol. Soc.*, 100, 1277–1298,
868 <https://doi.org/10.1175/BAMS-D-17-0278.1>, 2019.
- 869 Frau, F., Caboi, R., and Cristini, A.: The impact of Saharan dust on TMs solubility in rainwater in Sardinia, Italy, In:
870 *The Impact of Desert Dust Across the Mediterranean*, S. Guerzoni, and R. Chester (Eds.), Springer, Dordrecht, Environ.
871 *Sci. Technol. Library*, 11, 285–290, https://doi.org/10.1007/978-94-017-3354-0_28, 1996.
- 872 Fu, Y.F., Desboeufs, K., Vincent, J., Bon Nguyen, E., Laurent, B., Losno, R., and Dulac, F.: Estimating chemical
873 composition of atmospheric deposition fluxes from mineral insoluble particles deposition collected in the western
874 Mediterranean region, *Atmos. Meas. Tech.*, 10, 4389–4401, <https://doi.org/10.5194/amt-10-4389-2017>, 2017.
- 875 Fu, F., Desboeufs, K., Triquet, S., Doussin J.-F., Giorio C., Chevaillier S., Feron A., Formenti, F., Maisonneuve F.,
876 Riffaut, V.: Aerosol characterisation and quantification of trace element atmospheric dry deposition fluxes in remote
877 Mediterranean Sea during PEACETIME cruise, *Atmos. Chem. Phys.*, in prep.



- 878 Gallisai, R., Peters, F., Volpe, G., Basart., and Baldasano J. M.: Saharan Dust deposition may affect phytoplankton
879 growth in the Mediterranean S. Sea at ecological time scales, *PLoS One*, 9, e110762,
880 <https://doi.org/10.1371/journal.pone.0110762>, 2014.
- 881 Guerzoni, S, E Molinaroli, P Rossini, G Rampazzo, G Quarantotto, S Cristini.: Role of desert aerosol in metal fluxes in
882 the Mediterranean area, *Chemosphere*, 39, 229–246, [https://doi.org/10.1016/S0045-6535\(99\)00105-8](https://doi.org/10.1016/S0045-6535(99)00105-8), 1999b.
- 883 Guieu, C., and Ridame, C., Impact of atmospheric deposition on marine chemistry and biogeochemistry, in:
884 Atmospheric Chemistry in the Mediterranean - Vol. 2, From Air Pollutant Sources to Impacts, edited by Dulac, F.,
885 Sauvage, S., and Hamonou, E., Springer, Cham, Switzerland, in press, 2021.
- 886 Guieu, C., Chester, R., Nimmo, M., Martin, J. M., Guerzoni, S., Nicolas, E., Mateu, J., and Keyse, S.: Atmospheric
887 input of dissolved and particulate metals to the North Western Mediterranean, *Deep Sea Res. II*, 44, 655–674,
888 [https://doi.org/10.1016/S0967-0645\(97\)88508-6](https://doi.org/10.1016/S0967-0645(97)88508-6), 1997.
- 889 Guieu, C., Løye-Pilot, M. D., Ridame, C., and Thomas, C.: Chemical Characterization of the Saharan dust endmember:
890 Some biogeochemical implications for the Western Mediterranean Sea, *J. Geophys. Res.*, 107, 4258,
891 <https://doi.org/10.1029/2001JD000582>, 2002.
- 892 Guieu, C., Bonnet, S., Wagener, T., and Loÿe-Pilot, M.-D.: Biomass burning as a source of dissolved iron to the open
893 ocean?, *Geophys. Res. Lett.*, 32, L19608, <https://doi.org/10.1029/2005GL022962>, 2005.
- 894 Guieu, C, M.-D. Loÿe-Pilot, L. Benyahya, A. Dufour.: Spatial variability of atmospheric fluxes of metals (Al, Fe, Cd,
895 Zn and Pb) and phosphorus over the whole Mediterranean from a one-year monitoring experiment: Biogeochemical
896 implications, *Mar. Chem.*, 120, 164–178, <https://doi.org/10.1016/j.marchem.2009.02.004>, 2010.
- 897 Guieu, C., D'Ortenzio, F., Dulac, F., Taillandier, V., Doglioli, A., Petrenko, A., Barrillon, S., Mallet, M., Nabat, P., and
898 Desboeufs, K.: Introduction: Process studies at the air-sea interface after atmospheric deposition in the Mediterranean
899 Sea – objectives and strategy of the PEACETIME oceanographic campaign (May–June 2017), *Biogeosciences*, 17,
900 5563–5585, <https://doi.org/10.5194/bg-17-5563-2020>, 2020.
- 901 Hardy, J. T.: The sea surface microlayer: biology, chemistry and anthropogenic enrichment, *Prog. Oceanogr.*, 11, 307–
902 328, [https://doi.org/10.1016/0079-6611\(82\)90001-5](https://doi.org/10.1016/0079-6611(82)90001-5), 1982.
- 903 Heimbürger, L. E., Migon, C., Dufour, A., Chiffolleau, J. F., and Cossa, D.: Trace metal concentrations in the North-
904 western Mediterranean atmospheric aerosol between 1986 and 2008: Seasonal patterns and decadal trends, *Sci. Total*
905 *Environ.*, 408, 2629–2638, <https://doi.org/10.1016/j.scitotenv.2010.02.042>, 2010.
- 906 Heimbürger, A., Losno, R., Triquet, S., Dulac F., and Mahowald, N. M.: Direct measurements of atmospheric iron,
907 cobalt and aluminium-derived dust deposition at Kerguelen Islands, *Global Biogeochem. Cycles*, 26, GB4016,
908 <https://doi.org/10.1029/2012GB004301>, 2012.
- 909 Heimbürger, A., Losno, R., and Triquet, S.: Solubility of iron and other trace elements in rainwater collected on the
910 Kerguelen Islands (South Indian Ocean), *Biogeosciences*, 10, 6617–6628, <https://doi.org/10.5194/bg-10-6617-2013>,
911 2013.
- 912 Hersbach, H., Bell, B., Berrisford, P., Biavati, G., Horányi, A., Muñoz Sabater, J., Nicolas, J., Peubey, C., Radu, R.,
913 Rozum, I., Schepers, D., Simmons, A., Soci, C., Dee, D., Thépaut, J.-N.: ERA5 hourly data on single levels from 1979
914 to present, Copernicus Climate Change Service (C3S) Climate Data Store (CDS),
915 <https://doi.org/10.24381/cds.adbb2d47>, 2018.
- 916 Herut, B., Krom, M. D., Pan, G., and Mortimer, R.: Atmospheric input of nitrogen and phosphorus to the Southeast
917 Mediterranean: Sources, fluxes, and possible impact, *Limnol. Oceanogr.*, 44, 1683–1692,
918 <https://doi.org/10.4319/lo.1999.44.7.1683>, 1999.



- 919 Hydes, D.J., and Liss, P.S.: Fluorimetric method for the determination of low concentrations of dissolved aluminium
920 in natural waters, *Analyst*, 101, 922–931, 1976.
- 921 Gonzalez, L., and Briottet, X.: North Africa and Saudi Arabia day/night sandstorm survey (NASCube). *Remote Sens.*,
922 9, 896, <https://doi.org/10.3390/rs9090896>, 2017.
- 923 Izquierdo, R., Benítez-Nelson, C. R., Masqué, P., Castillo, S., Alastuey, A., Castillo, S., Alastuey, A., and Avila, A.:
924 Atmospheric phosphorus deposition in a near-coastal rural site in the NE Iberian Peninsula and its role in marine
925 productivity, *Atmos. Environ.*, 49, 361–370, <https://doi.org/10.1016/j.atmosenv.2011.11.007>, 2012.
- 926 Izquieta-Rojano, S., García-Gomez, H., Aguilhaume, L., Santamaría, J. M., Tang, Y. S., Santamaría, C., Valiño, F.,
927 Lasheras, E., Alonso, R., Ávila, A., Cape, J. N., and Elustondo, D.: Throughfall and bulk deposition of dissolved organic
928 nitrogen to holm oak forests in the Iberian Peninsula: flux estimation and identification of potential sources, *Environ.*
929 *Pollut.*, 210, 104–112, <https://doi.org/10.1016/j.envpol.2015.12.002>, 2016.
- 930 Jordi, A., Basterretxea, G., Tovar-Sánchez, A., Alastuey, A. and Querol, X.: Copper aerosols inhibit phytoplankton
931 growth in the Mediterranean Sea, *Proc. Nat. Acad. Sci.*, 109, 21246–21249, <https://doi.org/10.1073/pnas.1207567110>,
932 2012.
- 933 Kanakidou, M., Mihalopoulos, N., Kindap, T., Im, U., Vrekoussis, M., Gerasopoulos, E., Dermitzaki, E., Unal, A.,
934 Koçak, M., Markakis, K., Melas, D., Kouvarakis, G., Youssef, A. F., Richter, A., Hatzianastassiou, N., Hilboll, A.,
935 Ebojje, F., Wittrock, F., von Savigny, C., Burrows, J. P., Ladstaetter-Weissenmayer, A., and Moubasher, H.: Megacities
936 as hot spots of air pollution in the East Mediterranean, *Atmos. Environ.*, 45, 1223–1235,
937 <https://doi.org/10.1016/j.atmosenv.2010.11.048>, 2011.
- 938 Kanellopoulou, E. A.: Determination of heavy metals in wet deposition of Athens, *Global NEST J.*, 3, 45–50,
939 <https://doi.org/10.30955/gnj.000181>, 2001.
- 940 Longo, A. F., Ingall, E. D., Diaz, J. M., Oakes, M., King, L. E., Nenes, A., Mihalopoulos, N., Violaki, K., Avila, A.,
941 Benitez-Nelson, C. R., Brandes, J., McNulty, I., and Vine, D. J.: P-NEXFS analysis of aerosol phosphorus delivered to
942 the Mediterranean Sea, *Geophys. Res. Lett.*, 41, 4043–4049, <https://doi.org/10.1002/2014GL060555>, 2014.
- 943 Losno, R.: Chimie d'éléments minéraux en traces dans les pluies méditerranéennes, Ph.D. thesis, Univ. Paris-Diderot
944 de Paris 7, <https://tel.archives-ouvertes.fr/tel-00814327/document> (last accessed 4 July 2021), 1989.
- 945 Loÿe-Pilot, M.-D., and Martin, J. M.: Saharan dust input to the western Mediterranean: an eleven years record in
946 Corsica, , In: *The Impact of Desert Dust Across the Mediterranean*, Guerzoni, S., Chester, R. (Eds.), Springer,
947 Dordrecht, *Environ. Sci. Technol. Library*, 11, 191–199, https://doi.org/10.1007/978-94-017-3354-0_18, 1996.
- 948 Mackey, K. R. M., Buck, K. N., Casey, J. R., Cid, A., Lomas, M. W., Sohrin, Y., and Paytan, A.: Phytoplankton
949 Responses to Atmospheric Metal Deposition in the Coastal and Open-Ocean Sargasso Sea, *Front. Microbiol.*, 3, 359,
950 <https://doi.org/10.3389/fmicb.2012.00359>, 2012.
- 951 Mallet, M. D., D'Anna, B., Mème, A., Bove, M. C., Cassola, F., Pace, G., Desboeufs, K., Di Biagio, C., Doussin, J.-F.,
952 Maille, M., Massabò, D., Sciare, J., Zapf, P., di Sarra, A. G., and Formenti, P.: Summertime surface PM_j aerosol
953 composition and size by source region at the Lampedusa island in the central Mediterranean Sea, *Atmos. Chem. Phys.*,
954 19, 11123–11142, <https://doi.org/10.5194/acp-19-11123-2019>, 2019.
- 955 Markaki, Z., Loëe-Pilot, M. D., Violaki, K., Benyahya, L., and Mihalopoulos, N.: Variability of atmospheric deposition of
956 dis- solved nitrogen and phosphorus in the Mediterranean and possible link to the anomalous seawater N/P ratio,
957 *Mar. Chem.*, 120, 187–194, <https://doi.org/10.1016/j.marchem.2008.10.005>, 2010.
- 958 Migon, C., Robin, T., Dufour, A., and Gentili, B.: Decrease of lead concentrations in the Western Mediterranean
959 atmosphere during the last 20 years, *Atmos. Environ.*, 42, 815–821, <https://doi.org/10.1016/j.atmosenv.2007.10.078>,
960 2008.



- 961 Migon, C., Heimbürger-Boavida, L.-E., Dufour, A., Chiffolleau, J.-F., and Cossa, D.: Temporal variability of dissolved
962 trace metals at the DYFAMED time-series station, Northwestern Mediterranean, *Mar. Chem.*, 225, 103846,
963 <https://doi.org/10.1016/j.marchem.2020.103846>, 2020.
- 964 Milne, A., Landing, W., Bizimis, M., and Morton, P.: Determination of Mn, Fe, Co, Ni, Cu, Zn, Cd and Pb in seawater
965 using high resolution magnetic sector inductively coupled mass spectrometry (HR-ICP-MS), *Analytica Chimica Acta*,
966 665, 200–207, <https://doi.org/10.1016/j.aca.2010.03.027>, 2010.
- 967 Morel, F. M. M., Hudson, R. J. M., and Price, N. M.: Limitation of productivity by trace metals in the sea, *Limnol.*
968 *Oceanogr.*, 36, 1742–1755, <https://doi.org/10.4319/lo.1991.36.8.1742>, 1991.
- 969 Morel, F. M., Milligan, A. J., & Saito, M. A. Marine bioinorganic chemistry: the role of trace metals in the oceanic
970 cycles of major nutrients. *Treatise on geochemistry*, 6, 625, <https://doi.org/10.1016/B0-08-043751-6/06108-9>, 2003.
- 971 Morin, E., Krajeski, W. F., Goorich, D. C., Gao, X., and Sorooshian, S.: Estimating rainfall intensities from weather
972 radar data: The scale-dependency problem, *J. Hydrometeorol.*, 4, 782–797, [https://doi.org/10.1175/1525-7541\(2003\)004<0782:ERIFWR>2.0.CO;2](https://doi.org/10.1175/1525-7541(2003)004<0782:ERIFWR>2.0.CO;2), 2003.
- 974 Morley, N. H., Burton, J. D., Tankere, S. P. C., and Martin, J.-M.: Distribution and behaviour of some dissolved trace
975 metals in the western Mediterranean Sea, *Deep Sea Res. II*, 44, 675–691, [https://doi.org/10.1016/S0967-0645\(96\)00098-7](https://doi.org/10.1016/S0967-0645(96)00098-7), 1997.
- 977 Nehir, M., and Koçak, M.: Atmospheric water-soluble organic nitrogen (WSON) in the eastern Mediterranean: origin
978 and ramifications regarding marine productivity, *Atmos. Chem. Phys.*, 18, 3603–3618, <https://doi.org/10.5194/acp-18-3603-2018>, 2018.
- 980 Ochoa-Hueso, R., Allen, E. B., Branquinho, C., Cruz, C., Dias, T., Fenn, M. E., Manrique, E., Perez-Corona, M. E.,
981 Sheppard, L. J., and Stock, W. D.: Nitrogen deposition effects on Mediterranean-type ecosystems: an ecological
982 assessment, *Environ. Pollut.*, 159, 2265–2279, <https://doi.org/10.1016/j.envpol.2010.12.019>, 2011.
- 983 Özsoy, T., and Örnektekin, S.: TMs in Urban and Suburban Rainfall, Mersin, Northeastern Mediterranean, *Atmos. Res.*,
984 94, 203–219, <https://doi.org/10.1016/j.atmosres.2009.05.017>, 2009.
- 985 Pacyna, E. G., Pacyna, J. M., Fudala, J., Strzelecka-Jastrzab, E., Hlawiczka, S., Panasiuk, D., Nitter, S., Pregger, T.,
986 Pfeiffer, H., and Friedrich, R.: Current and future emissions of selected heavy metals to the atmosphere from
987 anthropogenic sources in Europe, *Atmos. Environ.*, 41, 8557–8566, <https://doi.org/10.1016/j.atmosenv.2007.07.040>,
988 2007.
- 989 Paris, R., and Desboeufs, K. V.: Effect of atmospheric organic complexation on iron-bearing dust solubility, *Atmos.*
990 *Chem. Phys.*, 13, 4895–4905, <https://doi.org/10.5194/acp-13-4895-2013>, 2013.
- 991 Pinedo-González, P., Joshua West, A., Tovar-Sánchez, A., Duarte, C. M., Marañón, E., Cermeño, P., González, N.,
992 Sobrino, C., Huete-Ortega, M., Fernández, A., López-Sandoval, D. C., Vidal, M., Blasco, D., Estrada, M., and Sañudo-
993 Wilhelmy, S. A.: Surface distribution of dissolved trace metals in the oligotrophic ocean and their influence on
994 phytoplankton biomass and productivity, *Global. Biogeochem. Cycles*, 29, 1763–1781,
995 <https://doi.org/10.1002/2015GB005149>, 2015.
- 996 Powell, C. F., Baker, A. R., Jickells, T. D., Bange, H. W., Chance, R. J., and Yodanis, C.: Estimation of the atmospheric
997 flux of nutrients and trace metals to the eastern tropical North Atlantic Ocean, *J. Atmos. Sci.*, 72, 4029–4045,
998 <https://doi.org/10.1175/JAS-D-15-0011.1>, 2015.
- 999 Pulido-Villena, E., Rérolle, V., and Guieu, C.: Transient fertilizing effect of dust in P-deficient LNLC surface ocean,
1000 *Geophys. Res. Lett.*, 37, L01603, <https://doi.org/10.1029/2009GL041415>, 2010.
- 1001 Pulido-Villena, E., Desboeufs, K., Djaoudi, K., Van Wambeke, F., Barrillon, S., Doglioli, A., Petrenko, A., Taillandier,
1002 V., Fu, F., Gaillard, T., Guasco, S., Nunige, S., Triquet, S., and Guieu, C.: Phosphorus cycling in the upper waters of



- 1003 the Mediterranean Sea (Peacetime cruise): relative contribution of external and internal sources, *Biogeosciences*
1004 *Discuss.*, <https://doi.org/10.5194/bg-2021-94>, in review, 2021.
- 1005 Rahn, K. A.: The Chemical Composition of the Atmospheric Aerosol, Tech. Rept., Graduate School of Oceanography,
1006 Univ. Rhode Island, Kingston, RI, 265 pp., <https://books.google.fr/books?id=q-dOQAAMAAJ> (last accessed 04 July
1007 2021), 1976.
- 1008 Raut, J.-C., and Chazette, P.: Assessment of vertically-resolved PM10 from mobile lidar observations, *Atmos. Chem.*
1009 *Phys.*, 9, 8617–8638, <https://doi.org/10.5194/acp-9-8617-2009>, 2009.
- 1010 Richon, C., Dutay, J.-C., Dulac, F., Wang, R., and Balkanski, Y.: Modeling the biogeochemical impact of atmospheric
1011 phosphate deposition from desert dust and combustion sources to the Mediterranean Sea, *Biogeosciences*, 15, 2499–
1012 2524, <https://doi.org/10.5194/bg-15-2499-2018>, 2018a.
- 1013 Richon, C., Dutay, J.C., Dulac, F., Wang, R., Balkanski, Y., Nabat, P., Aumont, O., Desboeufs, K., Laurent, B., Guieu,
1014 C., and Raimbault, P.: Modeling the impacts of atmospheric deposition of nitrogen and desert dust-derived phosphorus
1015 on nutrients and biological budgets of the Mediterranean Sea, *Prog. Oceanogr.*, 163, 21–39,
1016 <https://doi.org/10.1016/j.pocean.2017.04.009>, 2018b.
- 1017 Ridame, C., Le Moal, M., Guieu, C., TERNON, E., Biegala, I. C., L'Helguen, S., and Pujol-Pay, M.: Nutrient control of
1018 N₂ fixation in the oligotrophic Mediterranean Sea and the impact of Saharan dust events, *Biogeosciences*, 8, 2773–
1019 2783, <https://doi.org/10.5194/bg-8-2773-2011>, 2011.
- 1020 Royer, P., Chazette, P., Lardier, M., and Sauvage, L.: Aerosol content survey by mini N₂-Raman lidar: Application to
1021 local and long-range transport aerosols, *Atmos. Environ.*, 45, 7487–7495,
1022 <https://doi.org/10.1016/j.atmosenv.2010.11.001>, 2011.
- 1023 Rudnick, R. L., and Gao, S.: Composition of the Continental Crust. In: *Treatise on Geochemistry*, Holland, H. D., and
1024 Turekian, K. K. (Editors), Elsevier, Amsterdam. 3, 1–64, 2003.
- 1025 Saager, P. M., Schijf, J., and de Baar, H. J. W.: Trace-metal distributions in seawater and anoxic brines in the eastern
1026 Mediterranean Sea, *Geochim. Cosmochim. Acta*, 57, 1419–1432, [https://doi.org/10.1016/0016-7037\(93\)90003-F](https://doi.org/10.1016/0016-7037(93)90003-F),
1027 1993.
- 1028 Sandroni, V., and Migon, C.: Atmospheric deposition of metallic pollutants over the Ligurian Sea: labile and residual
1029 inputs, *Chemosphere*, 47, 753–764, [https://doi.org/10.1016/s0045-6535\(01\)00337-x](https://doi.org/10.1016/s0045-6535(01)00337-x), 2002.
- 1030 Saltikoff, E., Haase, G., Delobbe, L., Gaussiat, N., Martet, M., Idziorek, D., Leijnse, H., Novák, P., Lukach, M., and
1031 Stephan, K.: OPERA the Radar Project, *Atmosphere*, 10, 320, <https://doi.org/10.3390/atmos10060320>, 2019.
- 1032 Sciare, J., Bardouki, H., Moulin, C., and Mihalopoulos, N.: Aerosol sources and their contribution to the chemical
1033 composition of aerosols in the Eastern Mediterranean Sea during summertime, *Atmos. Chem. Phys.*, 3, 291–302,
1034 <https://doi.org/10.5194/acp-3-291-2003>, 2003.
- 1035 Sherrell, R. M. and Boyle, E. A.: Zinc, chromium, vanadium and iron in the Mediterranean Sea, *Deep Sea Res. A*, 35,
1036 1319–1334, [https://doi.org/10.1016/0198-0149\(88\)90085-4](https://doi.org/10.1016/0198-0149(88)90085-4), 1988.
- 1037 Smedley, P. L., and Kinniburgh, D. G.: Molybdenum in natural waters: A review of occurrence, distributions and
1038 controls, *Appl. Geochem.* 84, 387–432. <http://dx.doi.org/10.1016/j.apgeochem.2017.05.008>, 2017.
- 1039 Stortini, A. M., Cincinelli, A., Degli Innocenti, N., Tovar-Sánchez, A. and Knulst, J.: 1.12 - Surface Microlayer, In:
1040 *Comprehensive Sampling and Sample Preparation - Vol. 1: Sampling Theory and Methodology*, Pawliszyn, J. (Ed.-in-
1041 Chief), 223–246, Academic Press, Oxford, <https://doi.org/10.1016/B978-0-12-381373-2.00018-1>, 2012.



- 1042 Ternon, E., Guieu, C., Lojze-Pilot, M. D., Leblond, N., Bosc, E., Gasser, B., Miquel, J. C., Martin, J.: The impact of
1043 Saharan dust on the particulate export in the water column of the North Western Mediterranean Sea, *Biogeosciences*,
1044 7, 809–826, <https://doi.org/10.5194/bg-7-809-2010>, 2010.
- 1045 The Mermex Group, et al.: Marine ecosystems' responses to climatic and anthropogenic forcings in the Mediterranean,
1046 *Prog. Oceanogr.*, 91, 97–166, <https://doi.org/10.1016/j.pocean.2011.02.003>, 2011.
- 1047 Theodosi, C., Markaki, Z., Tselepidis, A., and Mihalopoulos, N.: The significance of atmospheric inputs of soluble and
1048 particulate major and TMs to the Eastern Mediterranean Sea, *Mar. Chem.* 120, 154–163,
1049 <https://doi.org/10.1016/J.MARCHEM.2010.02.003>, 2010.
- 1050 Thieuleux, F., Moulin, C., Bréon, F. M., Maignan, F., Poitou, J., and Tanré, D.: Remote sensing of aerosols over the
1051 oceans using MSG/SEVIRI imagery, *Ann. Geophys.*, 23, 3561–3568, <https://doi.org/10.5194/angeo-23-3561-2005>,
1052 2005.
- 1053 Tovar-Sánchez, A., Arrieta, J. M., Duarte, C. M., and Sañudo-Wilhelmy, S. A.: Spatial gradients in trace metal
1054 concentrations in the surface microlayer of the Mediterranean Sea, *Front. Mar. Sci.*, 1, 79,
1055 <https://doi.org/10.3389/fmars.2014.00079>, 2014.
- 1056 Tovar-Sánchez, A., González-Ortegón, E., and Duarte, C. M.: Trace metal partitioning in the top meter of the ocean,
1057 *Sci. Total Environ.*, 652, 907–914, <https://doi.org/10.1016/j.scitotenv.2018.10.315>, 2019.
- 1058 Tovar-Sánchez, A., Rodríguez-Romero, A., Engel, A., Zäncker, B., Fu, F., Marañón, E., Pérez-Lorenzo, M., Bressac,
1059 M., Wagener, T., Triquet, S., Siour, G., Desboeufs, K., and Guieu, C.: Characterizing the surface microlayer in the
1060 Mediterranean Sea: trace metal concentrations and microbial plankton abundance, *Biogeosciences*, 17, 2349–2364,
1061 <https://doi.org/10.5194/bg-17-2349-2020>, 2020.
- 1062 Van Wambeke, F., Taillandier, V., Deboeufs, K., Pulido-Villena, E., Dinasquet, J., Engel, A., Marañón, E., Ridame,
1063 C., and Guieu, C.: Influence of atmospheric deposition on biogeochemical cycles in an oligotrophic ocean system,
1064 *Biogeosciences Discuss.*, <https://doi.org/10.5194/bg-2020-411>, in review, 2020.
- 1065 Vincent, J., Laurent, B., Losno, R., Bon Nguyen, E., Rouillet, P., Sauvage, S., Chevaillier, S., Coddeville, P.,
1066 Ouboulmane, N., di Sarra, A. G., Tovar-Sánchez, A., Sferlazzo, D., Massanet, A., Triquet, S., Morales Baquero, R.,
1067 Fournier, M., Coursier, C., Desboeufs, K., Dulac, F., and Bergametti, G.: Variability of mineral dust deposition in the
1068 western Mediterranean basin and south-east of France, *Atmos. Chem. Phys.*, 16, 8749–8766,
1069 <https://doi.org/10.5194/acp-16-8749-2016>, 2016.
- 1070 Violaki, K., Bourrin, F., Aubert, D., Kouvarakis, G., Delsaut, N., and Mihalopoulos, N.: Organic phosphorus in
1071 atmospheric deposition over the Mediterranean Sea: An important missing piece of the phosphorus cycle, *Prog.*
1072 *Oceanogr.*, 163, 50–58, <https://doi.org/10.1016/j.pocean.2017.07.009>, 2018.
- 1073 Wagener, T., Pulido-Villena, E., and Guieu, C.: Dust iron dis-solution in seawater: Results from a one-year time-series
1074 in the Mediterranean Sea, *Geophys. Res. Lett.*, 35, L16601, <https://doi.org/10.1029/2008GL034581>, 2008.
- 1075 Wagener, T., Guieu, C., and Leblond, N.: Effects of dust deposition on iron cycle in the surface Mediterranean Sea:
1076 results from a mesocosm seeding experiment, *Biogeosciences*, 7, 3769–3781, <https://doi.org/10.5194/bg-7-3769-2010>,
1077 2010.
- 1078 Wurl, O.: *Practical Guidelines for the Analysis of Seawater*, 1st ed., CRC Press., 2009.
- 1079 Wuttig, K., Wagener, T., Bressac, M., Dammshäuser, A., Streu, P., Guieu, C., and Croot, P. L.: Impacts of dust
1080 deposition on dissolved trace metal concentrations (Mn, Al and Fe) during a mesocosm experiment, *Biogeosciences*,
1081 10, 2583–2600, <https://doi.org/10.5194/bg-10-2583-2013>, 2013.



1082 Yoon, Y. Y., Martin, J.-M., and Cotté, M. H.: Dissolved trace metals in the western Mediterranean Sea: total
1083 concentration and fraction isolated by C18 Sep-Pak technique, *Mar. Chem.*, 66, 129–148,
1084 [https://doi.org/10.1016/S0304-4203\(99\)00033-X](https://doi.org/10.1016/S0304-4203(99)00033-X), 1999.

1085

1086



1087 **Figure Captions:**

1088

1089 Figure 1: Total precipitation (mm) between May 28 at 20:00 UTC and 29 at 10:00 UTC from ERA5 ECMWF
1090 reanalysis. The red circle indicates the R/V position.

1091 Figure 2: On-board lidar-derived a) Apparent backscatter coefficient (ABC), (b) Temporal evolution (in
1092 Local Time) of the lidar-derived volume depolarization ratio (VDR) where the dust plume is highlighted for
1093 values higher than ~ 1.7 (yellow to red colors) and the rain by values higher than 3 (indicated by the arrow),
1094 and c) vertical profiles of the aerosol extinction coefficient (AEC) in cloud free condition, integrated over 3
1095 periods along the dust plume event, noted A, B and C in figure a. The grey shade represents the root mean
1096 square (rms) variability along the time of the measurement. The dust layer is highlighted on the profiles. The
1097 mean aerosol optical thickness is given in the boxed legend with its temporal variability (1 sigma). The
1098 location of the marine boundary layer (MBL) is also pointed.

1099 Figure 3: Rain rates (mm/h) during the night between the 4 and 5 June, when Rain Fast was collected on-
1100 board, issued from European rain radar composites (OPERA programme) of June 5 between 00:00 and 02:45
1101 UTC.

1102 Figure 4: Boxplots of dissolved (left panels) and particulate (right panels) marine concentrations (pM) for
1103 the different TMs within the ML (upper panels) and the SML (lower panels) at ION and FAST stations. In
1104 the box plots, the box indicates the interquartile range, i.e. the 25th and the 75th percentile, and the line within
1105 the box marks the median. The whiskers indicate the quartiles ± 1.5 times the interquartile range. Points above
1106 and below the whiskers indicate outliers outside the 10th and 90th percentile.

1107 Figure 5: Comparison of dissolved (D) and total (T) TMs concentrations along with data from 14 former
1108 studies carried out in the eastern and western Mediterranean Sea.

1109 Figure 6: Enrichment Factors (EF, upper panel) and solubility (% , bottom panel) of phosphorus (P) and TMs
1110 ordered by increasing EF in the two rainwater samples.

1111 Figure 7: Dissolved (upper panels) and particulate (lower panels) wet deposition fluxes ($\mu\text{mol m}^{-2}$) for the
1112 different TMs estimated from the two rains sampled on-board, considering the standard deviation on the TMs
1113 concentrations and the spatial variability of total precipitation over the area of sampling (Rain ION in blue
1114 and Rain FAST in red).

1115 Figure 8: Sampling chronology during the ION and FAST stations for SML, SSW and ML. The blue periods
1116 correspond to rainfall in the station area (after ERA 5 reanalysis and radar imagery, see section 3.1).
1117 Samplings were performed 4 days and 2 days before and 2 h after Rain ION, and at a higher frequency at the
1118 FAST station: 57, 37 and 7.5 hours before and 4.5, 12, 24 hours after Rain FAST. SML and SSW samples
1119 could not be collected immediately before and after the rains because of bad weather conditions, and were
1120 collected 3 and 4 days before Rain ION, and 57 and 20 h before and 30 h after Rain FAST.



1121 Figure 9: Comparison between TMs wet deposition fluxes (in green) and TMs marine stock delta (before
1122 and after the rain) in the SML (in blue) and in the ML (in red) at FAST. Dissolved = upper panels and
1123 particulate = lower panels. Marine stocks increase are expressed in absolute values (Cd, Co and Pb stocks in
1124 nmol m^{-2} , and the other TMs in $\mu\text{mol m}^{-2}$) and in relative values (%). N.E.: not enhanced (increase $<5\%$).

1125 Figure 10: Comparison of marine stocks in the ML at all the stations occupied during the PEACETIME
1126 cruise with atmospheric inputs estimated (1) from ION and FAST rains (Boxes) and (2) from an intense wet
1127 dust deposition event of 9 g m^{-2} (blue dots). Cd, Co and Pb stocks are in nmol m^{-2} , and the other TMs in
1128 $\mu\text{mol m}^{-2}$. For Mn, marine stocks are derived from surface concentrations close to Corsica coasts (Wuttig et
1129 al., 2013: samples OUT at 0, 5 and 10 m) and in the Ionian Sea (Saager et al., 1993: Bannock basin at 0, 10,
1130 and 15 m), as no measurement is available from the PEACETIME cruise. Boxes and whiskers as in Fig. 4.

1131